Robust and Adaptive Control Methods for Small Aerial Vehicles

by

Prasenjit Mukherjee

A thesis
presented to the University of Waterloo
in fulfillment of the
thesis requirement for the degree of
Master of Applied Science
in
Mechanical Engineering

Waterloo, Ontario, Canada, 2012

© Prasenjit Mukherjee 2012

I hereby declare that I am the sole author of this thesis. This is a true copy of the thesis, including any required final revisions, as accepted by my examiners.

I understand that my thesis may be made electronically available to the public.

Abstract

Recent advances in sensor and microcomputer technology and in control and aeroydynamics theories has made small unmanned aerial vehicles a reality. The small size, low cost and manoueverbility of these systems has positioned them to be potential solutions in a large class of applications. However, the small size of these vehicles pose significant challenges. The small sensors used on these systems are much noisier than their larger counterparts. The compact structure of these vehicles also makes them more vulnerable to environmental effects. This work develops several different control strategies for two sUAV platforms and provides the rationale for judging each of the controllers based on a derivation of the dynamics, simulation studies and experimental results where possible.

First, the coaxial helicopter platform is considered. This sUAV's dual rotor system (along with its stabilizer bar technology) provides the ideal platform for safe, stable flight in a compact form factor. However, the inherent stability of the vehicle is achieved at the cost of weaker control authority and therefore an inability to achieve aggressive trajectories especially when faced with heavy wind disturbances. Three different linear control strategies are derived for this platform. PID, LQR and H_∞ methods are tested in simulation studies. While the PID method is simple and intuitive, the LQR method is better at handling the decoupling required in the system. However the frequency domain design of the H_∞ control method is better at suppressing disturbances and tracking more aggressive trajectories.

The dynamics of the quadrotor are much faster than those of the coaxial helicopter. In the quadrotor, four independent fixed pitch rotors provide the required thrust. Differences between each of the rotors creates moments in the roll, pitch and yaw directions. This system greatly simplifies the mechanical complexity of the UAV, making quadrotors cheaper to maintain and more accessible. The quadrotor dynamics are derived in this work. Due to the lack of any mechanical stabilization system, these quadrotor dynamics are not inherently damped around hover. As such, the focus of the controller development is on using nonlinear techniques. Linear quadratic regulation methods are derived and shown to be inadequate when used in zones moderately outside hover. Within nonlinear methods, *feedback linearization* techniques are developed for the quadrotor using an inner/outer loop decoupling structure that avoids more complex variants of the feedback linearization methodology. Most nonlinear control methods (including feedback linearization) assume perfect knowledge of vehicle parameters. In this regard, simulation studies show that when this assumption is violated the results of the flight significantly deteriorate for quadrotors flying using the feedback linearization method. With this in mind, an adaptation law is devised around the nonlinear control method that actively modifies the plant parameters

in an effort to drive tracking errors to zero. In simple cases with sufficiently rich trajectory requirements the parameters are able to adapt to the correct values (as verified by simulation studies). It can also adapt to changing parameters in flight to ensure that vehicle stability and controller performance is not compromised. However, the direct adaptive control method devised in this work has the added benefit of being able to modify plant parameters to suppress the effects of external disturbances as well. This is clearly shown when wind disturbances are applied to the quadrotor simulations.

Finally, the nonlinear quadrotor controllers devised above are tested on a custom built quadrotor and autopilot platform. While the custom quadrotor is able to fly using the standard control methods, the specific controllers devised here are tested on a test bench that constrains the movement of the vehicle. The results of the tests show that the controller is able to sufficiently change the necessary parameter to ensure effective tracking in the presence of unmodelled disturbances and measurement error.

Acknowledgements

This thesis would not have been possible without the support and guidance of my supervisor, Professor Steven Waslander. His advice and experience informed much of the research direction and his constant encouragement was invaluable.

I would also like to thank my fellow lab mates at the Waterloo Autonomous Vehicles Lab: Arun Das, Neil Mathew, Yan Ma, John Daly, Mike Tribou, Yassir Rizwan, Peiyi Chen, Carlos Wang, Adeel Akhtar, Ryan Gariepy and Siddhant Ahuja. Their assistance on countless occasions has proven to be extremely important, and their company in the lab made the experience genuinely fun and interesting.

I am also grateful to the University of Waterloo Micro Aerial Vehicles Team, and especially members Derek Chow, Ryan Turner and Kyel Ok for their assistance in the design and construction of the custom made autopilot and quadrotor vehicle platform.

Finally, I would like to thank my family, who have supported me throughout.

Dedication

I dedicate this to my mother, father and sister, who have loved, supported and inspired me at every step of the way.

Table of Contents

List of Tables

List of Figures

Chapter 1

Introduction

The field of autonomous vehicles is a well developed and mature industry with numerous solutions to pressing problems. Within this industry, the field of unmanned and autonomous aerial vehicles (UAV) consists of a growing body of research that gives these systems access to terrain that was previously not drivable to their wheeled (or otherwise grounded) counterparts. Applications for this technology include remote surveillance, inspection, disaster reconnaissance, asset management, videography and many more. These possibilities have already shown significant market potential and as civilian skies open up to these systems, the market size is poised to grow to more than $94 Billion USD in the next decade [45].

In the last five to 10 years, small UAV systems (sUAV's, vehicles with less than 1 meter wing span) have become increasingly popular. This smaller scale is poised to advance the accessibility of these systems to areas previously deemed impossible to traverse by the traditionally larger aerial systems. This includes tight spaces such as indoors, forests, urban centers or natural caves. This miniaturization of aerial vehicles is further boosted by various factors,

- Low cost miniaturization of high performance computing platforms especially amplified by recent advances in the smartphone industry [2].
- Miniaturization of high performance sensor systems including IMU, GPS, RADAR and LIDAR systems
- The maturity of a large body of work in the comprehensive modelling of low reynolds number aerodynamics

- Breakthroughs in comprehensive analytical and computationally efficient modelling and control techniques

These factors together have created an excellent environment for sUAV technologies to be developed to the point of widespread application in various markets.

The fundamental problem with the safe operation of vehicles at a small ($< 1m$ wingspan) scale is reliable stabilization, robustness to unpredictable changes in the environment and resilience to noisy data from shrinking sensor systems. Autonomous operation of aerial vehicles relies upon on-board stabilization and trajectory tracking capabilities, and significant effort has to be made to make sure these systems are able to achieve stable flight. These problems are compounded at smaller scales as the vehicle is more susceptible to environmental effects (wind, temperature etc.). Moreover, the small scale implies that lower quality and noisier compact MEMS sensors are used as a primary sensor. The small form factor also makes it harder for the MEMS sensors to be isolated from the vibrations that are common in these flight platforms. As the number and complexity of applications for such systems grows daily, the control techniques involved must also improve to provide better performance and versatility.

Historically, simplistic linear control techniques were employed for computational ease and stable hover flight. However, with better modelling techniques and faster onboard computational capabilities, comprehensive nonlinear techniques to be run real-time have become an achieveable goal. Nonlinear methodologies promise to rapidly increase the possible flight envelope for these systems and make them more robust. However, they may not be universally applicable to all configurations of sUAV vehicle systems. Moreover, a vast majority of these nonlinear control methods require accurate knowledge of vehicle dynamics and therefore may be susceptible to any changes or inaccuracies therein.

This work presents control methods for two different sUAV configurations, the coaxial helicopter and the quadrotor helicopter. Choices of linear and nonlinear control methods are designed based on a comprehensive discussion of system dynamics. These methods are comparatively evaluated with simulations of real-world scenarios and operating modes for these flight systems. Finally, in this work a custom quadrotor and autopilot platform is developed. The nonlinear control methods are implemented on this system and the experimental results are evaluated.

1.1 Coaxial Helicopters

Coaxial helicopter systems were some of the first full-scale helicopters design and built [13]. A coaxial helicopter consists of a pair of counterrotating rotors that rotate about the same axis, thereby eliminating the need for a tail rotor to balance motor torque as in a conventional helicopter. This coaxial rotor configuration for a helicopter has numerous advantages especially at a smaller scale. As laid out in current literature [12], the advantages of the coaxial helicopter can be,

- **Inherent Stability**: Unlike a single rotor helicopter, the coaxial configuration is inherently stable due to its counter-rotating blades and stabilizer bar that are able to damp out sudden movements in attitude.
- **Power train efficiency**: The coaxial configuration has been shown to be upto 5% more efficient when compared to the single rotor or quad-rotor configurations [12, 13].
- **Speed Capabilities**: The single rotor helicopter has a fundamental disadvantage in that it has asymmetry of lift in forward flight [12]. This produces a varying amount of lift on the advancing and retreating half of the main rotor effectively imposing an upper limit on the forward speed. The coaxial helicopter overcomes this issue because there is always a pair of advancing and retreating blades. This configuration has allowed certain versions of the full scale coaxial helicopter to achieve forward flights of over 480 km/h [34].
- **Compact structure**: The coaxial helicopter does not require a tail-rotor to counteract the angular momentum of the main rotors. The counter-rotating rotors are used to counter-balance this moment. This makes the overall system more compact and lightweight. The resulting reduction in the moment of inertia significantly increases maneuverability [12].

Figure 1.1 shows some commercially available coaxial helicopter platforms along with some potential applications.

Despite these advantages, the coaxial helicopter design is not suitable for all applications. Being a rotorcraft, range and speed are limited relative to fixed wing designs, so applications requiring traversal of large distances with limited need for inspection are not suited to the coaxial helicopter. The twin rotors are more susceptible to wind disturbances over single rotor or quadrotor designs due to limited control authority, particularly in the small vehicle category. The design also favors stability over maneuverability, so that

agressive trajectories are difficult to achieve. Most coaxial systems are also mechanically complex. The system requires various mechanical linkages to actuate the aircraft and the coaxial configuration requires a more complex geartrain design making it costlier to maintain when compared to simpler designs such as the quadrotor. Ultimately, the efficiency and stability gains make coaxial helicopters ideal platforms for surveillance tasks requiring limited range and consistent perspective over moderate flight durations, but less than desirable for long distance or target tracking missions.

Much work has been done to develop models for coaxial platforms. The development of a precise dynamic model of the small coaxial helicopter was initiated by Bouabdallah et al. [37], which is one of the most complete models developed. Related efforts by Chen and McKerrow [12], Hendrix et al. [21], Wang et al. [39] and finally Dzul et al. [18] differ in the further assumptions made to help simplify the overall model. For example, Wang et al. [39] restrict their model to operating points close to hover conditions using small angle approximations earlier in the model derivation and Hendrix et al. [21] use a quadratic polynomial fit to thrust data in place of the usual thrust equation [9]. More critically, Hendrix et al. [21] and Bouabdallah et al. [37] are the only works that attempt to model the stabilizer bar movement (described in detail in Section 2.1) for controller design. Bouabdallah et al. [37] also identifies a scaling factor between the angle of the stabilizer bar and the angle of the upper rotor, while the work by Hendrix et al. [21] assumes this scaling factor to be unity. When designing controllers (see Section 2.2), Hendrix et al. [21] claims that dynamics between the upper rotor and the stabilizer bar can be sufficiently ignored to simplify the controller formulation. However, in the system identification procedure carried out by Bouabdallah et al., the stabilizer bar time constant was found to be 0.24s, and therefore not negligible for precision control. It is for this reason that the full model defined by Bouabdallah et al. [37] was used for the basis of controller formulation in this work.

A variety of linear multivarable controllers for the control of coaxial helicopter position, altitude and yaw is explored in this work. The four states (3D Position and Height) are considered critical in most missions with a focus on surveillance or data gathering. The above modeling techniques are used to investigate PID, LQR and H_∞ controller designs on a platform developed by the authors. All three controller designs are well established in the literature, with PID control on small coaxial helicopters first introduced by Watanabe et al. [40] and further developed by Wu et al. [43] using vision sensors. However, both works design and implement these controllers on conventional R/C helicopters with a few states already controlled by onboard electronics and no access to the actual platform actuators. Furthermore, the controllers are implemented off-board and only stable hover flight at a fixed location is considered. Hendrix et al. [21] consider full state feedback and optimal LQG control on coaxial platform. However, the authors only consider full

state feedback methods, which assume perfect state measurements based on IR optical methods, and perform all computations offboard. The controller designs by Schaforth et al. [37] are the only work that considers direct actuator control on the helicopter based on differential motor inputs and swashplate control. The work by Schaforth et al. [37] also considers robust control for the coaxial platform. This work intends to build on the work by Schaforth et al. [37] by introducing an alternate robust control structure, first suggested by Weilenmann et al. [41] for full-scale single rotor helicopters. A method of decoupling some of the cross-channel interaction for PID controller design is presented and optimal Linear Quadratic Regulation(LQR) control strategies with direct actuator control is also considered and compared.

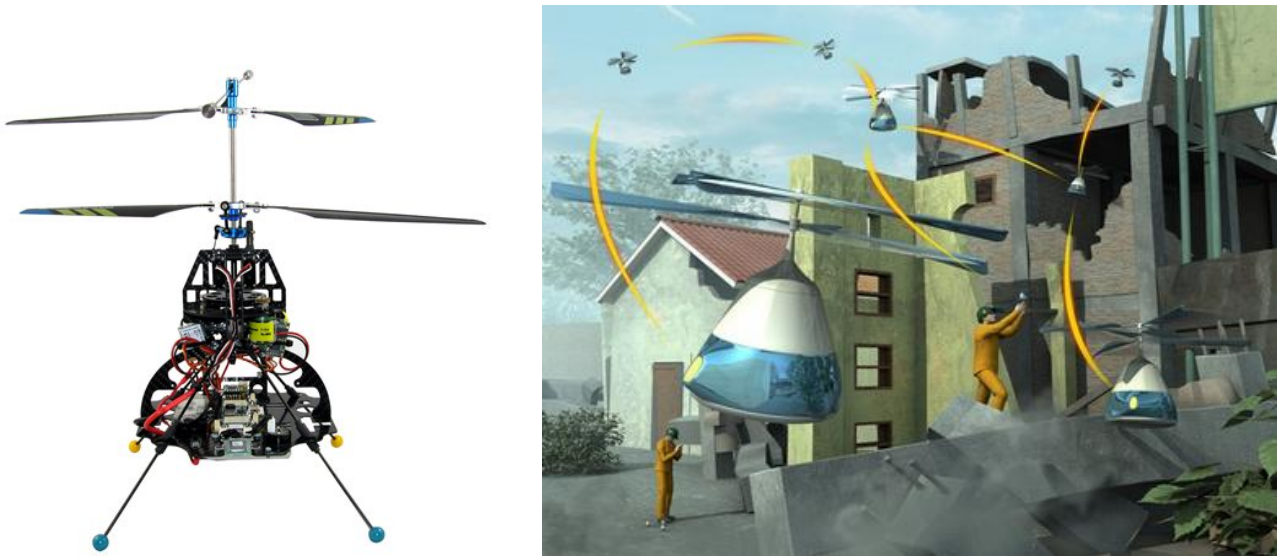

(a) Skybotix Coax Platform

(b) Artist Depiction of a Potential Coax Application (Courtesy: MuFly)

Figure 1.1: Coaxial Helicopter Platforms

1.2 Quadrotor Helicopters

The Quadrotor helicopter configuration is currently one of the most popular sUAV helicopter configurations. Four independent rotors are used to create the thrust and regulate the roll, pitch and yaw of the vehicle. This makes the mechanical design of the vehicle much

simpler. The quadrotor has numerous advantages that make it such a popular platform [22],

- **Mechanical Simplicity**: The quadrotor helicopter has fixed pitch rotors and four seperate rotor assemblies. This makes the system mechanically simple and therefore much easier and cheaper to maintain when compared to the coaxial and single rotor helicopters.
- **Smaller Rotor Size**: The quadrotor configuration uses four rotors which allows each rotor to be much smaller (for the same power output). This reduces the amount of kinetic energy in the system, alleviating the risk of major damage during a crash.
- **Control Authority**: Unlike the coaxial helicopter, the quadrotor system possesses substantial control authority i.e. the ability to apply signficant thrust for motion control. This enables the quadrotor helicopter to suppress the effect of various external disturbances and track aggressive trajectories.

Figure 1.2 shows a commercially available quadrotor platform along with a potential application currently under investigation.

However, just as in the case of a coaxial system, the quadrotor is unsuitable for long term flights. Moreover, the quadrotor aircraft does not have a mechanical system of damping the dynamics around hover, this means it has fast dynamics (velocities more 40km/h) that must be accurately controlled to ensure stability . While the coaxial helicopter is compact, the footprint of the quadrotor helicopter is larger for the same power output. Finally, unlike the coaxial helicopter, the quadrotor configuration does not naturally tend towards the linear flight regime (hover). This makes nonlinear control techniques more of a necessity to provide reliable and robust flight.

Quadrotor dynamics have been extensively investigated, with numerous models having been proposed which contain widely varying levels of fidelity and nonlinearity. The most comprehensive discussions can be found in work by Pounds et al. [33] and Hoffman et al. [23]. The work by Pounds [33] explores the effect of 'blade flapping' in quadrotor vehicles. Hoffman et al. [23] experimentally show the effect of blade flapping in their work and also explore various aerodynamic phenomenon that appear during flight at high velocities.

Numerous control methods have been proposed for quadrotors, for both regulation and trajectory tracking. The goal is to find a control strategy that allows the states of a quadrotor to converge to an arbitrary set of time-varying reference states. Many previous works [23, 14, 5, 33] have demonstrated that it is possible to control the quadrotor using

linear control techniques by linearizing the dynamics about an operating point, usually chosen to be around hover. However, a wider flight envelope and better performance can be achieved by using nonlinear control techniques that consider a more general form of the dynamics of the vehicle in all flight zones. Within these nonlinear methods, backstepping [28, 6], sliding mode [44, 6, 26] and feedback linearization [16] have been demonstrated to be effective with quadrotor control. Particularly, feedback linearization has shown significant promise for quadrotor vehicles. Position control using feedback linearization is theoretically impossible as the system has more output states than input signals. To get around this, *dynamic extension* is used to add virtual inputs to this system. The method of dynamic extension requires access to higher order derivative signals which have been shown to be too noisy in experimental studies [26]. However, recent work by Das et al. [16] suggests an alternate feedback linearization structure that deconstructs the quadrotor dynamics into an *inner loop* containing the attitude and height of the vehicle and an *outer loop* containing the position. The inner loop of the quadrotor platform is *square* i.e. it has the same number of inputs as ouputs. This means feedback linearization can be applied without the use of dynamic extension as long as the inverse of the dynamics exists in domain of interest. The outer loop can then be designed assuming arbitrary inner loop attitude requests can be achieved, which is feasible when relying on time scale separation between inner and outer loops, and with standard controllers acting on the integrator chains that result from the feedback linearization process. In general, this control structure shows significant promise and is investigated in this work along with linear methods such as LQR.

All the control techniques suggested above require complete knowledge of the system model and model parameters, but errors in the identified values of the parameters can lead to significant deterioration of the controller performance. Furthermore, unmodeled variations in system parameters (such as mass or inertia) during flight can cause significant stabilization errors to occur. The need for an accurate nonlinear model of quadrotor dynamics can be overcome by using adaptive methods that can react to and correct errors in model parameter estimates, modify parameter estimates when they change and also adjust for external disturbances. Linear adaptive methods such as Model Reference Adaptive Control (MRAC) have been suggested [42]. However, as for most linear methods, the achievable trajectory of the quadrotor is restricted due to the assumption of linearization. Some nonlinear adaptive methods such as adaptive sliding mode control [26] and adaptive backstepping [31] control have also been proposed. The work of Huang et al. [31] suggests an adaptive backstepping method, and this approach was extended to include inertia parameters in the adaptation law by Zeng et al. [46]. New work in autonomous grasping and construction using quadrotors also use indirect adaptive methods, such as the least-squares method (for mass) proposed by Kumar et al. [29]. However, all indirect

methods correct parameter errors based on the difference between the expected and actual plant outputs, but do not explicitly correct the model parameters to reduce tracking error (as done by direct adaptive methods). Direct adaptation methods were first suggested by Craig et al. [15] for mechanical manipulators. In this thesis, direct adaptive control is combined with feedback linearization to make up for some of the weaknesses of the pure feedback linearization approach. Finally, the work in nonlinear control design for quadrotor vehicles does not consider the effect of external disturbances on the controller performance, and yet disturbances such as wind gusts are commonly found in quadrotor operating environments. Models of wind disturbances commonly experienced by sUAV's are well known [32]. In this work, the dryden wind gust models are applied to the simulated dynamics to verify the performance of the suggested controllers.

(a) Aeryon Scout Platform

(b) Onboard imagery from a Quadrotor of Flare Stacks

Figure 1.2: Quadrotor Helicopter Platform and its potential uses

1.3 Research Approach and Contribution

This work considers two distinct sUAV platforms, the coaxial helicopter and the quadrotor helicopter. Chapter 2 presents the different features of coaxial helicopter dynamics. The coaxial helicopter design with flybar is passively stable, and tends to its nominal hover condition, about which linear models are sufficiently accurate for control design. As a result, PID, LQR and H_∞ techniques can be applied, as has been demonstrated in the literature [37, 8, 21]. The H_∞ controller design proposed in this work builds on similar efforts applied

to single rotor vehicles [41]. Chapter 2 also presents comprehensive simulation studies that directly compares the performance of the various controllers. The effect of environmental disturbances on these controllers is also presented.

Section 3 contains a comprehensive discussion of quadrotor dynamics as derived in various current works. Quadrotor dynamics do not exhibit the same passive stability characteristic of the coaxial design, and therefore, quadrotors are more natural candidates for nonlinear control methods. In this work, a linear LQR controller for the quadrotor is developed as a baseline for comparison to various nonlinear methods. H_∞ controllers and nonlinear control methods are equally complex. Moreover, the linearity assumption (required by H_∞) is frequently violated in flight. Therefore, robust linear methods are not considered for quadrotors. Instead, the design focus is on feedback linearization and adaptive feedback linearization methods based on an inner loop/outer loop control structure. Again, the performance of all the controllers is evaluated in a simulated environment in the presence of enviromental disturbances. Experimental results for both LQR control and feedback linearization on quadrotors can be found in recent literature [7, 26]. However, experimental results for adaptive feedback linearization methods have not been presented before. Section 4 contains a description of the custom autopilot and quadrotor platform that is constructed for nonlinear control tests. Section 4 also contains the experimental results that verify's the advantages of the nonlinear methods described in Section 3. In summary, the main novel contributions that will be presented in this thesis are:

- A new H_∞ controller is designed using the robust mixed synthesis method. This design uses a new set of frequency domain constrains derived from the specific requirements of the coaxial helicopter. While a similar control strategy was used for large scale single rotor helicopters [41], a controller with this design has never been tried on a coaxial system.

- A comprehensive simulation study that shows the specific advantages and disadvantages of PID, LQR and the new H_∞ controller. While these controllers have been independently developed by others, they have never been directly compared. This comparison will aid future designers in making a more informed decision about the controllers available to them.

- A traditional feedback linearization method is improved upon by the addition of adaptive elements that continously correct the parameters used by the feedback linearization method. This adaptation is shown to reduce tracking errors in various scenarios when compared to the results of a traditional feedback linearization method.

- As in the case of the coaxial helicopter, the feedback linearization method, LQR controller and the adaptive elements are directly compared under various scenarios.
- A custom autopilot platform is built and installed on an open source quadrotor platform. This platform is then used to test the feedback linearization controller in real-time. Using the autopilot platform, the advantages of the adaptive elements suggested in this work is experimentally shown.

Chapter 2

Coaxial Helicopter Dynamics and Control

Autonomous flight of small coaxial helicopters poses significant challenges in terms of comprehensive yet computationally feasible modeling and control. The coaxial platform provides several advantages at small scales in terms of size, footprint, efficiency and stability. This study compares techniques used for the modeling and control of such an aircraft in order to identify a viable control design for an experimental platform. Models of the various thrust and motor dynamics are presented, and the fidelity of the model is assessed. In terms of control techniques, linear methods such as PID, LQR and H_∞ mixed synthesis are presented. Simulation results of the control methods developed here are presented in Section 2.3.

2.1 Flight Dynamics

2.1.1 Basic Flight Principles

The flight of a small radio-controlled coaxial helicopter is commonly controlled through four main actuators, the two main blades (rotors) and two servos that control the orientation (roll and pitch) of the lower rotor through a swash-plate. A diagram with the basic mechanical layout is shown in Figure 2.1. Most commercially available remote controlled coaxial helicopter platforms have fixed pitch rotors, as such the rest of the model is defined using this assumption. This model can be extended to systems with collective and cyclic pitch control if required.

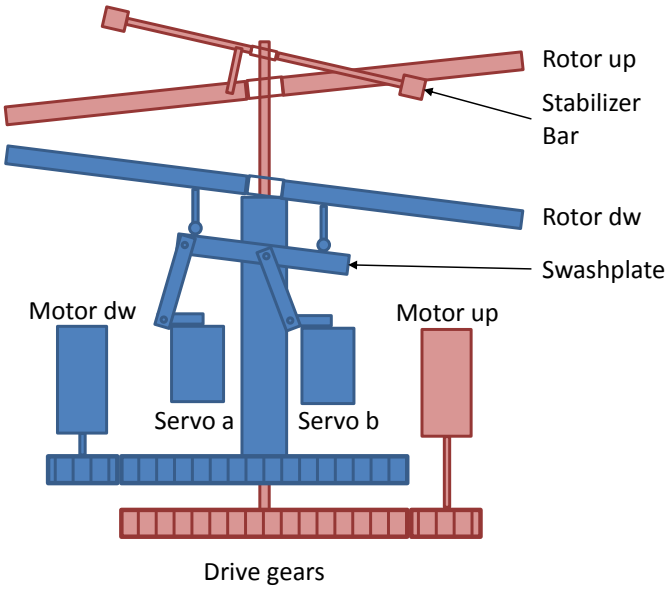

Figure 2.1: Actuators on a Coaxial Helicopter

The main thrust in the system is provided by the two main rotors. The altitude is controlled by varying the rotational speeds of both rotors. The rotational torques generated by turning the two rotors are in opposite directions which keeps the yaw of the system stable, and can be varied to provide yaw control. The roll and pitch of the vehicle are controlled by varying the orientation of the rotor hub, which tilts the tip path plane causing the thrust direction to shift. This actuation is achieved by tilting a swashplate using two servos, one for roll and one for pitch.

The change in the direction of thrust causes translational forces in the longitudinal and lateral directions and a moment about the center of gravity. Along with the four actuators there is commonly a passive input provided by a stabilizer bar that dampens any movements in the roll and pitch directions. Such an assembly is shown in Figure 2.2. The stabilizer bar provides a redress moment as it guides the upper rotor to follow the lower rotors' roll and pitch movements with dynamics commonly modeled as a first order lag [21, 37]. This redress moment keeps the system inherently stable.

Figure 2.2: Stabilizer Bar on Bell 212/HH-1N rotor head. Photo: Alan K. Radecki (CC BY-SA 3.0)

2.1.2 Coordinate Systems

As is typical with aerospace applications [20], the NED inertial coordinate frame will be used, and denoted by *X, Y, Z*. For body coordinates, *x, y, z* will be used, as depicted in Figure 2.3. To transform between coordinate frames, a rotation matrix $R \in SO(3)$ is defined, along with 3-2-1 Euler angles $\phi, \theta, \psi \in [0, 2\pi)$ such that

$$\begin{bmatrix} X \\ Y \\ Z \end{bmatrix} = R \begin{bmatrix} x \\ y \\ z \end{bmatrix}, \tag{2.1}$$

where the rotation matrix R can be expressed in term of Euler angles as,

$$R = \begin{bmatrix} c\phi c\psi & -c\phi s\psi + s\phi s\theta c\psi & s\theta s\psi + c\phi s\theta c\psi \\ c\theta s\psi & c\phi c\psi + s\phi s\theta s\psi & -s\phi c\psi + c\phi s\theta s\psi \\ -s\theta & s\phi c\theta & c\phi c\theta \end{bmatrix} \tag{2.2}$$

The Euler angles ϕ, θ, ψ constitute the Roll, Pitch and Yaw of the vehicle respectively. The rotations of the helicopter are represented using Euler angles instead of unit quaternions because gimbal lock is not considered to be an issue with the manoeuvres involved in the control of coaxial helicopters. The notation $c\phi$, $s\phi$, $t\phi$ is used to denote $\cos\phi$, $\sin\phi$, and $\tan\phi$, respectively.

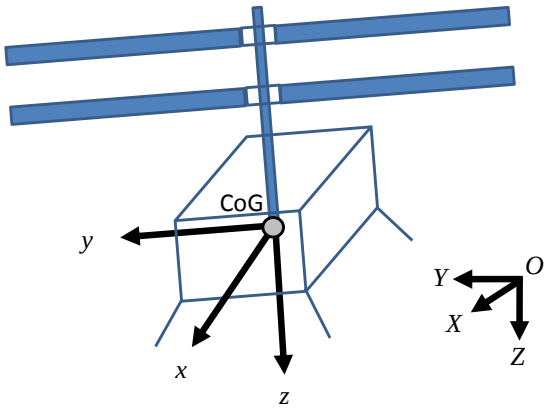

Figure 2.3: *xyz* and *NED*/XYZ frames.

Similarly, to transform angular rate quantities from body coordinates p, q, r (rad/s) to Euler angle rates, the matrix C is used such that

$$\begin{bmatrix} \dot{\phi} \\ \dot{\theta} \\ \dot{\psi} \end{bmatrix} = C \begin{bmatrix} p \\ q \\ r \end{bmatrix} \tag{2.3}$$

where $C \in \mathbb{R}^{(3\times3)}$ is defined as,

$$C = \begin{bmatrix} 1 & t\theta s\phi & t\theta c\phi \\ 0 & c\phi & -s\phi \\ 0 & \frac{s\phi}{c\theta} & \frac{c\phi}{c\theta} \end{bmatrix} \tag{2.4}$$

2.1.3 Equations of Motion

To capture the motion of the vehicle due to forces and moments, the general 6 DOF equations for a moving body are used. The equations for translational acceleration in the body frame as per [20, 30] are,

$$\begin{bmatrix} \ddot{x} \\ \ddot{y} \\ \ddot{z} \end{bmatrix} = \frac{1}{m}\vec{F} - \vec{\omega} \times \vec{v} \tag{2.5}$$

Similarly, for angular rates using the Inertia tensor $I \in \mathbb{R}^{(3\times3)}$ the equations guiding the angular moments can be expressed as,

$$\begin{bmatrix} \dot{p} \\ \dot{q} \\ \dot{r} \end{bmatrix} = I^{-1}(\vec{M} - \vec{\omega} \times I\vec{\omega}) \tag{2.6}$$

The above equations now define the motion of the helicopter in generalized co-ordinates using external forces and torques. These external inputs must now be defined with respect to the dynamics of the helicopter.

2.1.4 Forces and Moments

Three main forces $\vec{F}$ acting on the vehicle are considered,

- A force of gravity acting on the center of gravity
- Thrust forces due to the rotors
- Downwash and aerodynamic interaction between the two coaxial rotors

The center of gravity of the system is assumed to be aligned with the body z-axis. The force of gravity acting on the body in the inertial frame is assumed to be on the inertial Z axis with magnitude mg. The direction of this vector can be quantified in the body co-ordinates using the transpose of Eqn. (2.1) as

$$\vec{e_g} = \begin{bmatrix} -s\theta \\ s\phi c\theta \\ c\phi c\theta \end{bmatrix} \tag{2.7}$$

In terms of the magnitude of the thrust generated by the individual blades, aerodynamic theory suggests [9]

$$F_i = \frac{\rho C_l U^2 S}{2} \tag{2.8}$$

where, ρ is the density of air, S is the surface area of the blade, i $\in up, down$, U is the induced velocity and C_l is the lift coefficient. It is possible to assume that the induced velocity is proportional to the rotor rate of rotation (steady state assumption),

$$F_i = k_i \omega_i^2 \tag{2.9}$$

where i signifies the top or bottom rotor on the coaxial helicopter and ω_i is rotor speed. Since the rotor pitch is fixed, the value of k_i cannot be varied in flight, as is possible with a variable pitch rotor. Instead, thrust is modulated by changing the rate of rotation of the rotor.

The final forces under consideration are the downwash on the vehicle body and the aerodynamic interaction of the two rotor system. Bouabdallah et al. [37] were able to identify a small but significant downwash force (at a constant 0.0108N), while the effect of the interaction of the two rotors is mostly ignored. That is, the effect of the downwash of the top rotor on the freestream velocity observed by the bottom rotor is not independently modeled but is instead lumped into different thrust coefficients for the two rotors and modeled as essentially constant throughout the flight envelope.

Force Directions

Longitudinal and lateral acceleration are primarily achieved through deflection of the rotor plane. The fixed pitch tip path plane control method is used primarily on small coaxial helicopters, where it is considered sufficiently capable to control the vehicle. The direction of the thrust can be resolved into two perpendicular vectors α and β that can be used to express the angle of the rotor hub and the resultant tip path plane. These vectors are shown in Figure 2.4 with respect to the body frame.

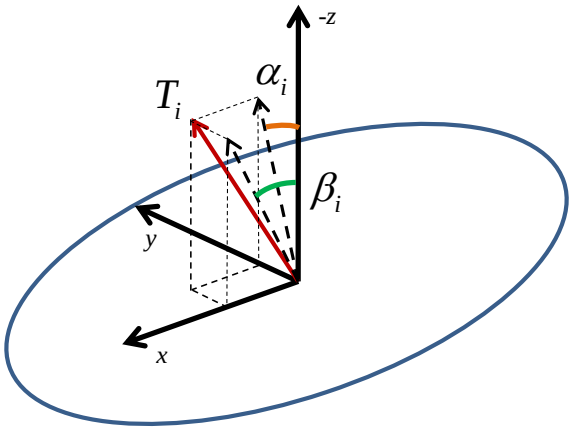

Figure 2.4: α_i and β_i for each rotors tip path plane

The swash-plate angles (α_{dw} and β_{dw}) are directly controlled by independent servos and lead to the unit vector [37] of the rotor plane normal,

$$\hat{e}_{dw} = \begin{bmatrix} \cos\alpha_d w \sin\beta_d w \\ \sin\alpha_d w \\ -\sin\alpha_d w \cos\beta_d w \end{bmatrix} \tag{2.10}$$

Therefore, the total force from the lower rotor would be, as per Eq. (2.9),

$$\vec{F}_{dw} = k_{dw}\omega_{dw}^2 \hat{e}_{dw} \tag{2.11}$$

While the above equations describe the force direction for the lower rotor, the upper rotor has an independent force direction. The top rotor is coupled to a stabilizer bar and has slower transients that keep the overall system stable. Similar to the lower rotor hub, the stabilizer bar tip path plane can be quantified using the angles α_s and β_s. The stabilizer bar dynamics can be described as [37],

$$\dot{\alpha_s} = \frac{1}{T_{stab}}(\phi - \alpha_s) \tag{2.12}$$

$$\dot{\beta_s} = \frac{1}{T_{stab}}(\theta - \beta_s) \tag{2.13}$$

The stabilizer bar angles lag behind any changes in the roll and pitch causing the redress moment that keeps the vehicle stable. This lag is represented using the first order lag equation shown in Eqn (2.12) and (2.13). The stabilizer bar angles are then transferred to body coordinates and linearly scaled to express the angles of the top rotor hub, which controls the thrust direction.

$$\begin{aligned} \alpha_{up} &= k_{stab}(\alpha_s - \phi) \\ \beta_{up} &= k_{stab}(\beta_s - \theta) \end{aligned} \tag{2.14}$$

Based on these angles the direction of the thrust vector can be realised as per Eqn. (2.10) and the total force from the upper rotor is defined analogously to Eqn. (2.11). Therefore, the total force generated on the helicopter in body co-ordinates is,

$$\vec{F} = \vec{F}_{up} + \vec{F}_{dw} + mg\hat{e}_g \tag{2.15}$$

Once the forces and their corresponding directions are established, the equations guiding the generation of the moments ($\vec{M}$) can be gathered from two sources,

- A misalignment between the forces in Eqn. (2.15) and the body z-axis
- Aerodynamic reaction torques applied on the central rotor hub due to the rotor velocities

The misalignment between the body forces and the body z-axis are due to nonzero thrust directions (α_i and β_i). The forces causing moments about the center of gravity act at the rotor hubs. The distance between the rotor hub and the center of gravity is quantified here as the vector $\vec{z}_i$ where $i \in up, dw$. Thus, the moments due to this misalignment can be expressed [37, 39, 18] as,

$$\vec{M}_{al} = \vec{z}_{up} \times \vec{e}_{up} F_{up} + \vec{z}_{dw} \times \vec{e}_{dw} F_{dw} \tag{2.16}$$

The aerodynamic reaction torques can be expressed [37] as a function of the rotational velocity of the rotors,

$$M_{ae} = c_Q^{up} \pi \rho R^5 \omega_{up}^2 + c_Q^{dw} \pi \rho R^5 \omega_{dw}^2 = k_q^{up} \omega_{up}^2 + k_q^{dw} \omega_{dw}^2 \tag{2.17}$$

where, once again, $i \in up, dw$. Note that as a simplifying assumption, the aerodynamic reaction torques are assumed to act solely about the body z-axis. Thus, the total moments acting on the body can be quantified as,

$$\begin{aligned} \vec{M} &= \vec{M}_{al} + \vec{M}_{ae} \\ &= \vec{z}_{up} \times F_{up} \vec{e}_{up} + \vec{z}_{dw} \times F_{dw} \vec{e}_{dw} + k_{q,up} \omega_{up}^2 \hat{z} + k_{q,dw} \omega_{dw}^2 \hat{z} \end{aligned} \tag{2.18}$$

The coaxial helicopter system also experiences gyroscopic torques as a result of combined motion in the roll or pitch and the yaw direction [12]. This is a nonlinearity that is present when experiencing a yaw moment during extreme roll and/or pitch motion which the coaxial helicopter is not expected to experience. As a result, this phenomenon is not considered in this work. This simplification has been made in numerous works about coaxial helicopters. [37, 21, 37].

2.1.5 Actuator Transients

The inputs used to define the forces and moments in the dynamic model have been assumed to be α_{dw}, β_{dw}, ω_{up} and ω_{dw}. However, these inputs are derived from actuators that have transients that must be considered. It is possible to consider the standard DC motor model to quantify these transients [21] as,

$$J_m \dot{\omega} = -b\omega + K_t I - \tau \tag{2.19}$$

$$L\dot{I} = -RI - K_e\omega + V \tag{2.20}$$

where, J_m is the motor inertia K_t and K_e are electrical constants, L is the circuit inductance, R is the armature resistance, τ is the generated motor torque, ω is the motor speed and V and I are the input voltage and current respectively. However, this model can be simplified by assuming a linear relationship between the electronic input and the motor speed and armature current. This removes the requirement to track motor transients and also reduces the size of the state to be controlled. However, this is done at the expense of a higher fidelity motor model

The servos that control the swashplate are modeled as having a first order lag and a linear mapping. This is done as,

$$\dot{X}_{dw} = \frac{1}{T_{f,dw}}(-l_{dw}u_{s,i}\theta_S - X_{dw}) \tag{2.21}$$

where $X \in (\alpha, \beta)$ can be either servo actuating both rotor path angles, $u_{s,i}$ is the electronic servo input (arbitrarily scaled), $T_{f,dw}$ is the time constant guiding the first order lag, l_{dw} is a linear mapping between the swashplate angle and the rotor angle and θ_S is the maximum swashplate angle. Furthermore, it is also possible to model the rotor transients as a function of input voltage, gear train efficiencies, frictional losses and aerodynamic back torques [37],

$$J_m\dot{\omega}_i = \frac{k_m U_{bat} u_{mot,i} - k_m k_e i_g \omega_i}{i_g R_\omega} - d_r\omega_i - \frac{c_{q,i}k_{q,i}\omega_i^2}{i_g^2\eta_g} \tag{2.22}$$

where J_m, k_m, k_e, R_ω are the motor constants as described before, i_g and η_g are the gear ratio and gear efficiencies respectively, U_{bat} is the full battery voltage, and the last term is simply based on the aerodynamic back torque as per Eq. (2.17).

Here it must be noted that the time constant guiding the servo transients ($T_{f,dw}$) can be extremely fast (as little as 0.001s [37]). This small time constant for the servo transient can be removed from the model without significant detriment to the system model [21, 39]. However, the rotor transients cause a significant time delay that is often ignored [21, 39]. Since the rotor speed is used to control the altitude of the aircraft, the rotor speed delay may cause less than ideal altitude controller performance. As such, in this work the motor time delay is included into the model by making motor speeds (ω_{up} and ω_{dw}) a part of the state. In summary, the equations of motion that sufficiently capture the motion of a coaxial helicopter with inputs $u = \begin{bmatrix} \alpha_{dw} & \beta_{dw} & u_{mot,up} & u_{mot,dw} \end{bmatrix}$ are,

$$\begin{bmatrix} \ddot{x} \\ \ddot{y} \\ \ddot{z} \end{bmatrix} = \frac{1}{m}\vec{F} - \vec{\omega} \times \vec{v} \tag{2.23}$$

$$\begin{bmatrix} \dot{p} \\ \dot{q} \\ \dot{r} \end{bmatrix} = I^{-1}(\vec{M} - \vec{\omega} \times I\vec{\omega}) \tag{2.24}$$

where,

$$\vec{F} = \vec{F}_{up} + \vec{F}_{dw} + mg\hat{e}_g \tag{2.25}$$

$$\vec{F}_{dw} = k_{dw}\omega_{dw}^2\hat{e}_{dw} \tag{2.26}$$

$$\vec{F}_{up} = k_{up}\omega_{up}^2\hat{e}_{up} \tag{2.27}$$

$$\vec{M} = \vec{z}_{up} \times F_{up}\vec{e}_{up} + \vec{z}_{dw} \times F_{dw}\vec{e}_{dw} + k_{q,up}\omega_{up}^2\hat{z} + k_{q,dw}\omega_{dw}^2\hat{z} \tag{2.28}$$

The motion of the force vectors can be characterized with,

$$\hat{e}_{dw} = \begin{bmatrix} \cos\alpha_{dw}\sin\beta_{dw} \\ \sin\alpha_{dw} \\ -\sin\alpha_{dw}\cos\beta_{dw} \end{bmatrix} \tag{2.29}$$

$$\hat{e}_{up} = \begin{bmatrix} \cos\alpha_{up}\sin\beta_{up} \\ \sin\alpha_{up} \\ -\sin\alpha_{up}\cos\beta_{up} \end{bmatrix} \tag{2.30}$$

$$\alpha_{up} = k_{stab}(\alpha_s - \phi) \tag{2.31}$$

$$\beta_{up} = k_{stab}(\beta_s - \theta) \tag{2.32}$$

$$\dot{\alpha}_s = \frac{1}{T_{stab}}(\phi - \alpha_s) \tag{2.33}$$

$$\dot{\beta}_s = \frac{1}{T_{stab}}(\theta - \beta_s) \tag{2.34}$$

Finally, the speed of the motors can be characterized with,

$$J_m\dot{\omega}_{up} = \frac{k_m U_{bat} u_{mot,up} - k_m k_e i_g \omega_{up}}{i_g R_\omega} - d_r\omega_{up} - \frac{c_{q,up}k_{q,up}\omega_{up}^2}{i_g^2\eta_g} \tag{2.35}$$

$$J_m\dot{\omega}_{dw} = \frac{k_m U_{bat} u_{mot,dw} - k_m k_e i_g \omega_{dw}}{i_g R_\omega} - d_r\omega_{dw} - \frac{c_{q,dw}k_{q,dw}\omega_{up}^2}{i_g^2\eta_g} \tag{2.36}$$

2.2 Control Techniques

2.2.1 Linearization

As is common in helicopter control and necessary for the linear control methods described below, the plant is linearized about the hover operating point. The coaxial helicopter dynamics are designed to ensure the plant always tends towards this hover point to keep the system stable. This means that the coaxial design favors stability and tighter control over faster, wider and more aggressive trajectory tracking (such as flips and high angle of attack maneuvers) and makes the coaxial platform favourable for flight in tight spaces. An important advantage of this tendency towards damping hover flight is that it makes the linearization about hover a reasonable and reliable assumption.

The plant state is first divided into three main components as illustrated in Figure 2.5.

- Throttle/Yaw Plant: Upper and lower motors ($u_{mot,up}$ and $u_{mot,dw}$) controlling the throttle (affecting altitude) and yaw of the plant.
- Y Position (Roll) Plant: Lower Swashplate Angle(α_{dw}) controlling the Roll (and Y position) of the plant
- X Position (Pitch) Plant: Lower Swashplate Angle(β_{dw}) controlling the Pitch (and X position) of the plant

It is noted here that the three plants have minimal cross-channel interaction in the full non-linear plant when linearized about hover. The linearization is a Taylor series approximation of the nonlinear equations shown in Section 2.1.3, with the higher order terms ignored as the plant is sufficiently close to the equilibrium point of hover. This approximation is derived by calculating the Jacobian of the nonlinear functions around the prescribed state. This linearization results with the three plants with states as follows,

Throttle/Yaw Plant

$$x = \begin{bmatrix} z & \dot{z} & \psi & r & \omega_{up} & \omega_{dw} \end{bmatrix}^T \tag{2.37}$$

Roll/Y Direction Plant

$$x = \begin{bmatrix} y & \dot{y} & \theta & q & \zeta_{bar} \end{bmatrix}^T \tag{2.38}$$

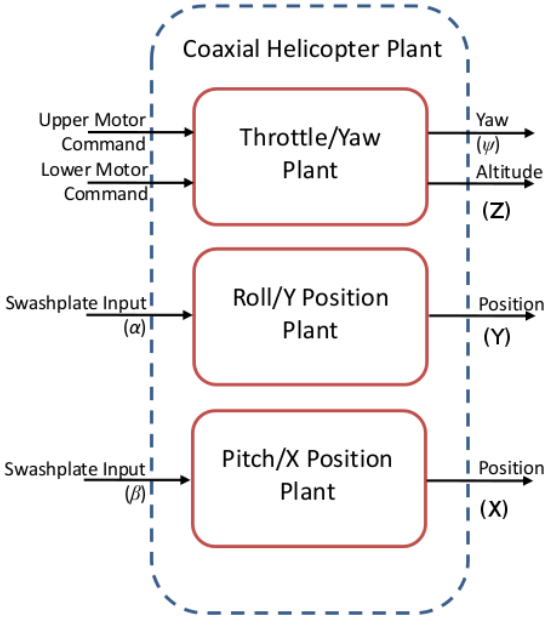

Figure 2.5: Linearized Sub-Plants

Pitch/X Direction Plant

$$x = \begin{bmatrix} x & \dot{x} & \phi & p & \eta_{bar} \end{bmatrix}^T \tag{2.39}$$

The position and velocity variables in the above states are kept in local co-ordinates. This can be transformed to inertial co-ordinates using complete attitude information when required. With these plants the controllers can now be designed. A sample set of plant parameters are used to aid in the simulation studies.

2.2.2 PID Control

Some of the earliest techniques applied to small coaxial helicopters involved simple PID or PD loops assuming near linear behaviour in hover conditions [43, 40]. Multi-loop PID

control techniques were used to first stabilize the helicopter in hover using PD control on the attitude of the vehicle and then track positions using PID control with the attitude as the output of the controller. This basic layout is shown in Figure 2.6.

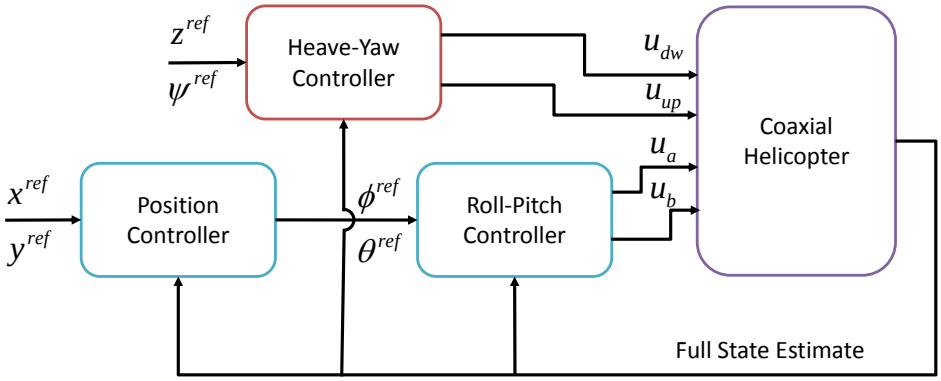

Figure 2.6: General PID Loop layout.

Both PID control methods shown in current literature [43, 40] are successful in achieving hover flight, and remain close to the point of linearization. However, the performance of the helicopter in complex trajectories or the evidence of cross-channel interaction is not shown. Furthermore, in all PID controller designs, the helicopters have had stock R/C chassis controllers and stabilizers present within the loop. This includes yaw rate regulators and throttle controllers abstracted out for easier pilot control. As such, the controller designs have used the yaw rate and throttle controllers as inputs. However, in most applications of autonomous coaxial systems the inputs would be the electronic control of the two motors affecting the throttle and yaw of the helicopter (as previously discussed in Section 2.1.1).

With this in mind, PID controllers are designed using the inputs and controller structure laid out in Figure 2.6 for the sub-plants shown in Figure 2.5. PID controllers for the throttle and yaw of the helicopter are designed first. As described before, the throttle of most coaxial helicopters are controlled by changing the speed of the two rotors (changing the total thrust). The yaw of the vehicle is controlled by a difference in the speed of the two rotors. This coupled behaviour between the throttle and yaw of the vehicle must first be removed for PID control to be effective. This is done by constructing two PID controllers that generate a thrust control signal and a yaw control signal based on the errors of the respective states. The yaw control signal is applied to the two motors *differentially* so as to minimize any effect on the total throttle. The throttle signal is applied equally to both motors to minimize any effect on the yaw rate of the helicopter. This decoupling is illustrated in Figure 2.7.

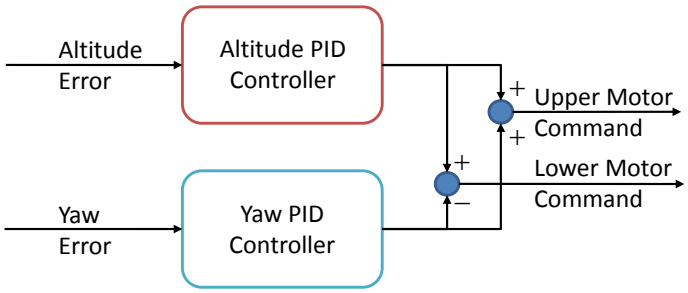

Figure 2.7: Altitude/Yaw PID Decoupling

This decoupling allows the PID loops to be tuned and used separately. However, this structure assumes that the upper motor and lower motor signals have an equal effect on the two rotors and therefore on the total thrust and aerodynamic reaction torques. This will most likely be untrue on most coaxial helicopters due to the extra inertia of the stabilizer bar on the upper rotor and the downwash of the upper rotor which affects the lower rotor freestream velocity. These effects were not considered in the design of the PID control structure. The PID controller is tested in simulation with the results of a step input to both altitude (1 m rise in altitude) and yaw (1 rad $\approx 60°$) presented in Figure 2.8.

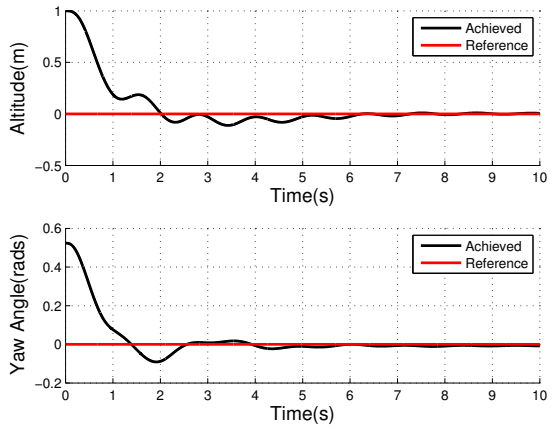

Figure 2.8: Altitude/Yaw PID results

As is clear from Figure 2.8, the decoupling strategy is able to effectively stabilize the system, however, the performance is less than desirable. This is mostly due to the cross-channel effects compounded by the asymmetry of torque generated by the two motors

(included in the simulation). A better tuned PID controller may be possible, but the inherent weakness of ignoring the interaction between yaw and altitude remains.

For position control, a tilt in the tip path plane causes a change in the roll and pitch of the vehicle and a tilt of the total thrust vector in the x and/or y direction. The input to the tilt of the tip path plane are the two servo inputs α_{dw} and β_{dw} affecting the roll/y position and the pitch/x position systems, respectively. The stabilizer bar design tends to return the roll and pitch of the vehicle towards zero. As such, these attitude commands do not need to be actively controlled or stabilized. However, for tighter PID position control it is more effective to have closed loop roll and pitch control. The overall order of the open loop plant, which translates servo inputs to position, is 5^{th} order, which makes it difficult for any PID controller to achieve acceptable transient performance. With this in mind, two PID controllers are designed for position control in each axis. There is minimal cross-channel interaction between the controllers for the two axes, and they can be individually tuned. The result of a step input in the x-direction is shown in Figure 2.9.

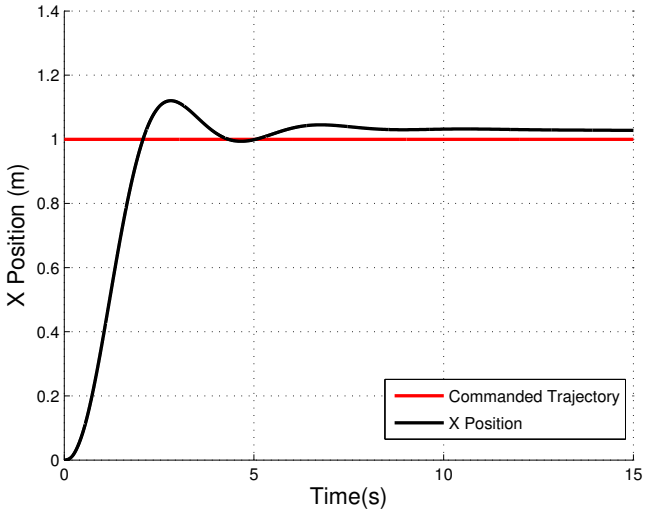

Figure 2.9: Position PID results

The plot shows that the controller is able to stabilize the position of the vehicle. Furthemore, saturators in the simulation ensured that no more than a 10° roll and pitch is commanded of the vehicle to ensure the stabilizer bar can effectively keep the attitude of the vehicle stable around hover. A constant error is seen in the plot. This consant error could be due to inherent nonlinearities in the system that the PID structure is unable to

remove. Stronger integral action could remove this error faster, however this could lead to more 'ringing' in the position which is undesirable for a platform to be used in small spaces.

For more complex position, altitude and yaw trajectories and comparative results between all three controllers presented in this section, see Section 2.3.

2.2.3 LQR/LQG Control

Full state feedback control using optimal control techniques has been shown to be effective in MIMO systems with significant cross-channel interaction [10]. With this in mind, a static gain LQR controller is constructed for a sample coaxial helicopter [8]. A similar LQR controller has been constructed by Hendrix et al. [21], along with a Kalman filter for state estimation. However, just as in the case of the existing PID designs, the LQG controller is designed for an R/C platform with built-in yaw, throttle, roll and pitch control. Furthermore, complex position trajectories are not analyzed. As described in detail in Skogestad et al. [38], LQR/LQG control works to generate a control signal $u(t)$, which minimizes the quadratic cost function based on the state feedback $x(t)$,

$$J_r = \int \big(x(t)^T Q x(t) + u(t)^T R u(t)\big) dt \tag{2.40}$$

This can be done with a control signal, $u(t) = Kx(t)$, calculated by

$$K = R^{-1} B^T X \tag{2.41}$$

where X is calculated using the algebraic Ricatti equation,

$$A^T X + XA - XBR^{-1}B^T X + Q = 0 \tag{2.42}$$

which can be solved using several mathematical computing software packages. The matrices Q and R in the above equations are weighting matrices that provide information about the relative importance of each state and input respectively. Also, note here that the LQR control strategy assumes full state feedback. State estimators can be used to handle noisy sensor measurements and incorporate details about the model (eg. LQG control).

LQR controllers are designed for each of the three sub-plants shown above using Q and R matrices that favour precise tracking of the altitude, yaw and x-y position states and weight all inputs equally. The matrices are also scaled to ensure they use a nominal

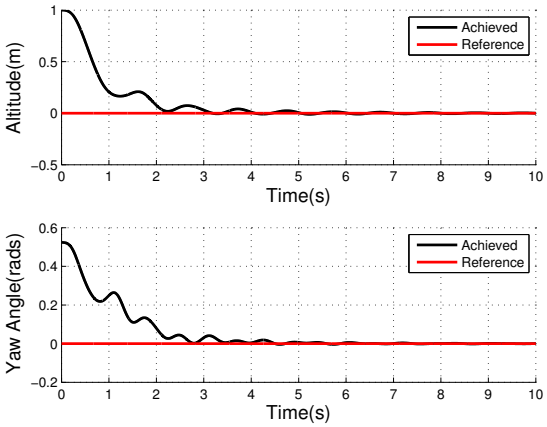

Figure 2.10: Altitude/Yaw results using LQG Control

amount of control effort. Based on this design, simulation results are shown in Figure 2.10 and Figure 2.11, for the Altitude/Yaw and Position sub-plants, respectively.

In Figure 2.10, the cross-channel interaction is shown to be completely mitigated, especially when compared to the PID results shown in Figure 2.8 for the same plant. The controller actively takes into account the lack of symmetry in both plants and is shown to remove its effects.

Figure 2.11 shows results of position control using the LQG controller. The controller is able to converge to the required trajectory much faster than in PID control. For explicitly comparative results and results of the frequency domain analysis and complex trajectories, see Section 2.3.

2.2.4 H_∞ Control

While LQR control strategies provide good cross-channel interaction suppression and can provide good transient characteristics, they do not allow for the direct design of the frequency domain properties. This includes the shaping of the system response at different frequencies and guaranteed phase margins [17]. LQG control with dynamic weightings using the H_2 norm has been suggested as an alternative that provides more frequency domain control. However, current results on full-sized single-rotor helicopters by Weilenmann et al. [41] show that H_∞ control can provide superior results. For this, mixed sensitivity H_∞ techniques are employed to design the frequency domain characteristics of a controller for

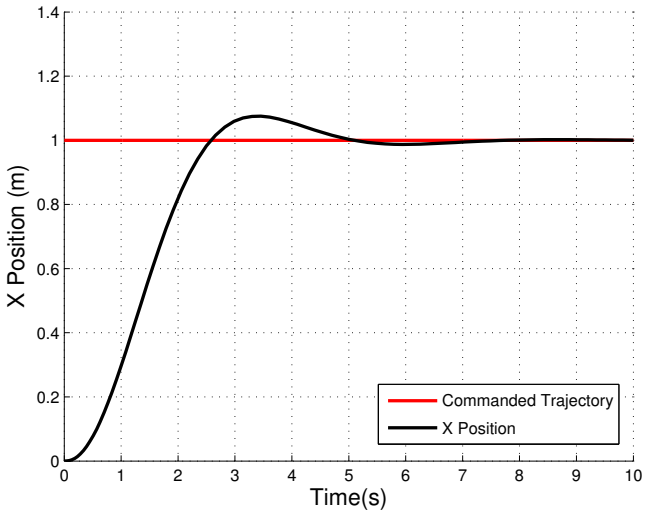

Figure 2.11: Position control using LQG control

the sample coaxial platform as before [8]. A more comprehensive description of the mixed synthesis design theory and process can be found in Skogestad et al. [38]. In traditional mixed synthesis design, the sensitivity ($S = \frac{1}{1+KP}$ with K the controller and P the plant), complementary sensitivity ($T = I - S$) and control effort (KS) functions are shaped to be under some bounds prescribed in the frequency domain. These functions represent the tracking error suppression (and disturbance rejection), target tracking (and sensor noise rejection) and bounds on the control effort in a wide range of frequencies. The bounds (namely W_p, W_u, W_y) are defined to ensure the controller satisfies the inequalities,

$$||S|| \leq \left|\left|\frac{1}{W_p}\right|\right|, \quad ||KS|| \leq \left|\left|\frac{1}{W_u}\right|\right|, \quad ||T|| \leq \left|\left|\frac{1}{W_y}\right|\right| \tag{2.43}$$

The above equations can then be rearranged to be,

$$||W_p S|| \leq 1, \quad ||W_u KS|| \leq 1, \quad ||W_t T|| \leq 1 \tag{2.44}$$

The mixed synthesis problem is then framed as an H_∞ norm optimization problem by stacking the three inequalities above,

$$\min_{K} \left\| \begin{matrix} W_p S \\ W_T T \\ W_u K S \end{matrix} \right\|_\infty \tag{2.45}$$

Note, however, that this structure for the design of H_∞ controllers cannot be used with non-square systems, that is systems that do not have the same number of inputs and outputs. An alternative design based on Weilenmann et al. [41] is proposed that includes a feedforward term. This structure will further aid in the tight control of reference trajectories due to the feedforward struture, which is especially important for precise position control in small spaces. A modifiction of the Weilenmann et al. structure is illustrated in Figure 2.12.

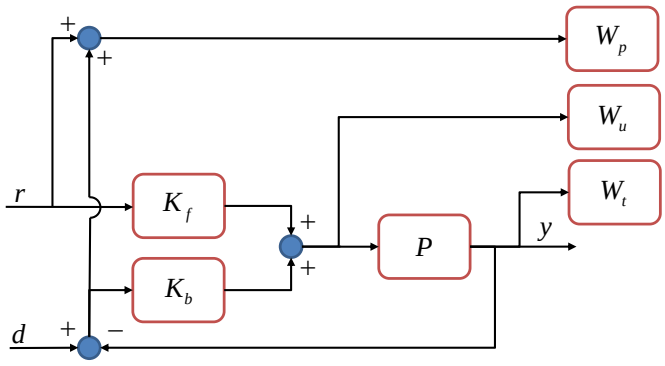

Figure 2.12: Proposed H_∞ structure

The H_∞ structure proposed in Figure 2.12 assumes a reference trajectory, r, plant output y and output disturbance, d. More dynamic weights to shape the effect of disturbances and reference signals can be added if required. With this structure, the minimization described in Eqn. (2.45) remains the same and an extra degree of freedom in the controller design is added. The gain K_f is the dynamic feedforward gain while the gain K_b is the dynamic feedback gain as shown in Figure 2.12. The weight W_p is picked to minimize the tracking error at low frequencies as shown in the resultant magnitude plot in Figure 2.13.

$$W_p = \frac{s + 0.0007}{s + 7} \tag{2.46}$$

This also translates to effective disturbance rejection at these frequencies. Similarly, W_t is picked as,

$$W_t = \frac{0.001s + 10}{s + 7} \tag{2.47}$$

which attempts to ensure a high gain response of the reference trajectory tracking at lower frequencies and a fast roll-off after the bandwidth (≈ 7 rad/s) to ensure good sensor noise rejection at high frequencies. The magnitude response of this is shown in Figure 2.13.

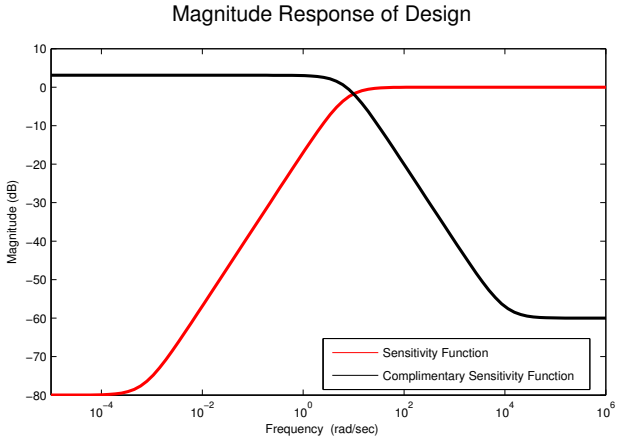

Figure 2.13: Magnitude plot for H_∞ design bounds

The bounds shown in Figure 2.13 are applied to all channels and used for both the throttle/yaw and position sub-plants. The weight W_u depends on the scaling of the inputs and the plant, it is picked to be < 1 to let the control effort be managed efficiently. The H_∞ norm optimization problem shown in Eqn.(2.45) can now be solved using thesse bounds to provide an effective controller. This can be done with built in tools in most popular mathematical computing packages. The controller design results must satisfy (or come close to) the inequality shown in Eqn.(2.44). A commonly used measure of optimality here is γ which is the distance of the achieved controller closed loop response from the bounds shown in Figure 2.13. This value is confirmed to be close to unity (i.e. no difference). However, the exact value of γ will depend on the particulars of the plant.

The controllers acquired from the H_∞ norm optimization process are applied to the plants as before. Figure 2.14 shows the result of a unit step reference commanded of the H_∞ controller for throttle/yaw sub-plant (as done before for the other controllers). It is clear that the controller is able to stabilize the plant and also results in faster response times than the PID and LQR controllers (see Section 2.3 for comparisons).

Figure 2.15 shows the tracking of a unit step position command where fast and stable tracking of position commands can be seen.

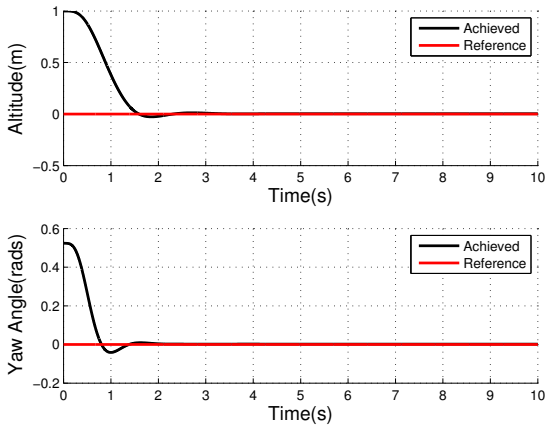

Figure 2.14: Altitude and Yaw control using H_∞ control

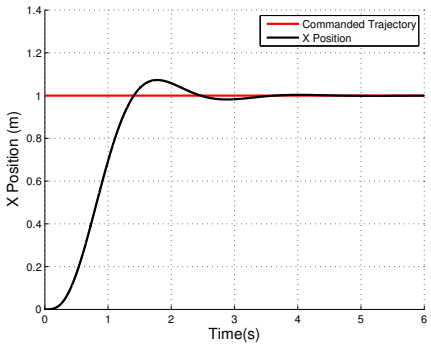

Figure 2.15: X Position tracking using H_∞ control

2.3 Comparitive Results

Figure 2.16 shows the unit step responses for the three controllers. The PID controller results have a significant 'ringing' due to the cross-channel effects and platform restrictions. LQR and H_∞ control provide good results, with H_∞ resulting in the fastest response times with an acceptable amount of overshoot.

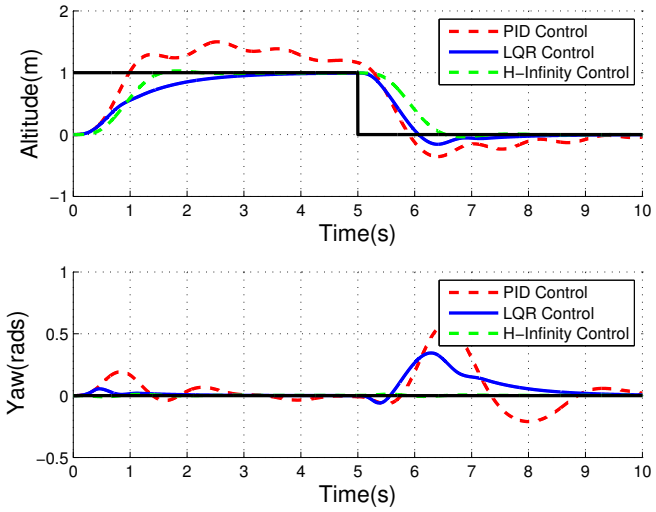

Figure 2.16: Heave and Yaw Unit step tracking

A similar response can be seen in Figure 2.17, where the H_∞ controller outperforms the LQR and PID controllers in unit step position tracking with LQR control providing acceptable results.

Furthermore, to test the overall robustness of the controllers, a variant of the Dryden wind gust model [19] is applied to the relevant states as wind disturbances. The Dryden wind gust model mathematically defines the affect of wind gusts on an aircraft. It generates an approximation of wind gusts by summing wind velocities over a pre-defined freqency power spectra. The model then generates an approximation of the forces experienced by a flight craft based on the wind speed and the speed of the aircraft with respect to the free stream velocity. A simplification of the Dryden model is simulated for this work. A force vector is generated based on the sum of wind velocities over a pre-defined frequency. This force is applied as a disturbance on the dynamics of the aircraft as a simulation of the affect of wind. The response under these conditions on the altitude of the system is shown in

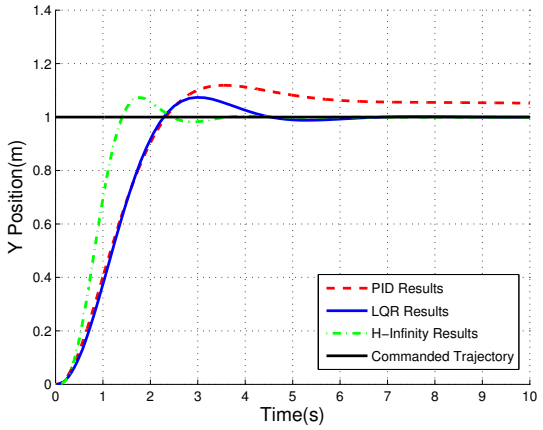

Figure 2.17: Position Unit Step Tracking for all controllers

Figure 2.18, which demonstrates the system is able to maintain stability and performance for all three controllers. However, for the PID control strategy, the disturbance in the altitude also affects the performance of the yaw controller because of the coupling effects previously mentioned. The LQR and H_∞ controllers are able to actively supress these cross-channel interferences.

The coaxial platform is more susceptible to disturbances in the X and Y position plane because of the lower inertia in this direction (when compared to the altitude states). This is evident in Figure 2.19, where the wind disturbance is applied to the helicopter in the x direction. The PID controller results show significant degradation as expected. However, the LQR and H_∞ controllers continue to perform well. Here, it could be hypothesized that the H_∞ controller should perform better than LQR control in disturbance rejection, however the controller design's focus is on better performance in tight spaces (versus disturbance rejection in wide open spaces). Furthermore, the coaxial platform has a fundamental physical limitation in that it is far more susceptible to external disturbances and is much slower to react to the same when compared to other rotorcraft configurations. This limitation may be causing the inability of the H_∞ controller to perform more ably under external disturbances.

In the following simulations, a changing reference trajectory (sinusoid) is applied to each of the controllers. The resulting trajectory is shown in Figure 2.20. Here, both the LQG and PID controllers show significant degradation in performance, while the H_∞ controller is still able to perform with an acceptable amount of error at this frequency. A practical application of this improved response at different frequencies is the tracking of

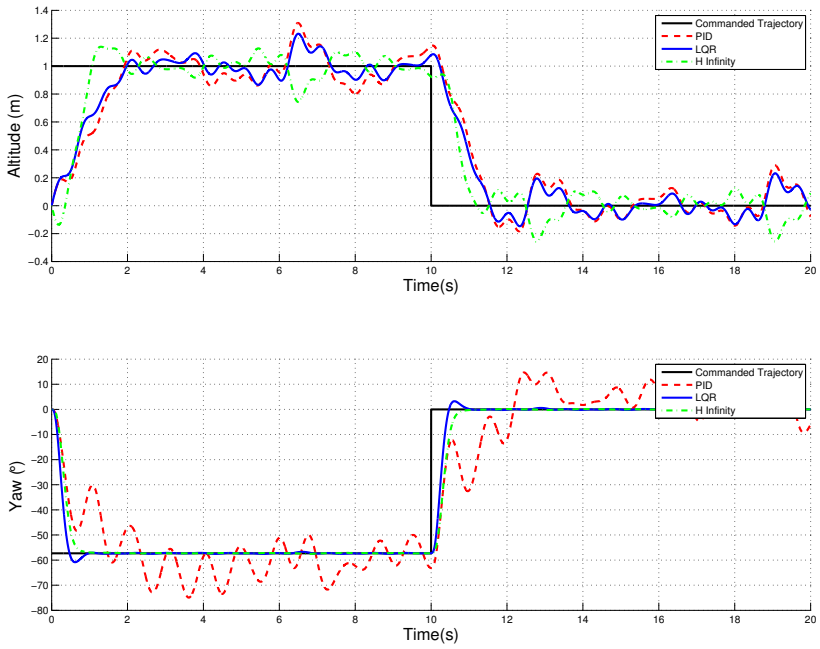

Figure 2.18: Altitude and Yaw under scaled Wind Disturbance

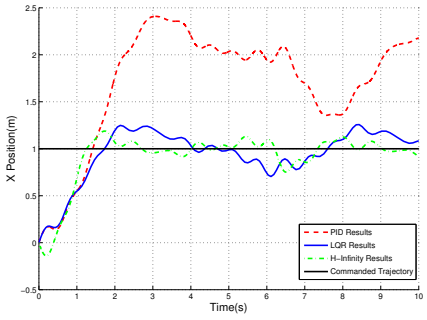

Figure 2.19: Position Control under scaled Wind Disturbance

aggressive and tight trajectories that require the helicopter to respond to fast changing reference signals. This is especially useful for maneouvering in small spaces with speed and accuracy. A sample of such an aggressive multivariable trajectory is shown in Figure 2.21.

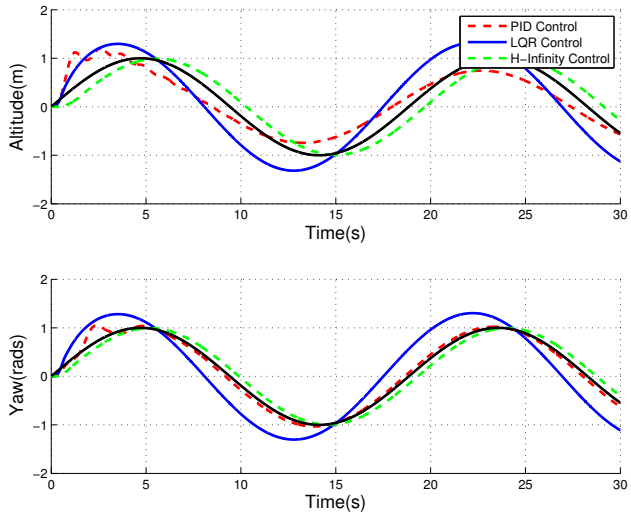

Figure 2.20: Sinusoidal Trajectory Tracking with Degrading PID/LQG performance

The H_∞ controller is able to very accurately track the given trajectory while the LQR and PID controllers provide less desirable results. In summary, the PID controller is able to stabilize the coaxial helicopter dynamics however the controller is unable to suppress various nonlinearities in the system. The LQR controller is able to control the helicopter with better results. However, the frequency domain design of H_∞ is shown to be superior in suppressing the various nonlinearties, and performs better when required to track an aggressive trajectory or suppress external disturbances.

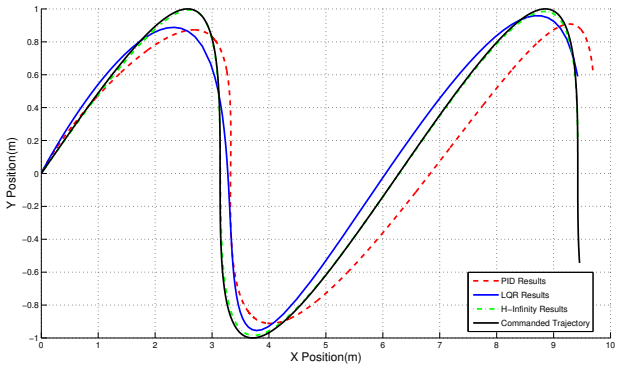

Figure 2.21: Aggressive 2D Trajectory Tracking

Chapter 3

Quadrotor Helicopter Dynamics and Control

The four rotor helicopter configuration is a popular UAV/MAV platform in the <1m wingspan category. Along with a simpler mechanical design, quadrotor systems have a unique set of dynamics that allow for holonomic flight which makes it suitable for flight in tight spaces such as indoors, forests, urban centers or natural cave environments. In this work, the dynamics of the quadrotor helicopter are derived and include most major factors that affect the motion of quadrotors. Furthermore, a combination of linear, nonlinear and adaptive control methods are presented for the quadrotor vehicle.

3.1 Flight Dynamics

3.1.1 Basic Flight Principles

Basic quadrotor dynamics are well understood and various derivations can be found in literature [23, 4, 33]. The quadrotor helicopter is a VTOL aircraft that can be controlled by four main rotors that provide an upward thrust. The rotors spin in clockwise and counter clockwise directions in pairs so that the resultant torque created can be controlled to keep the yaw angle of the system stable. Similarly, by reducing or increasing the thrust generated by each rotor, the roll and pitch of the vehicle can be controlled. This also provides control of the overall thrust vector which can be used to control the position of the helicopter. A freebody diagram for this is shown in Figure 3.1(a).

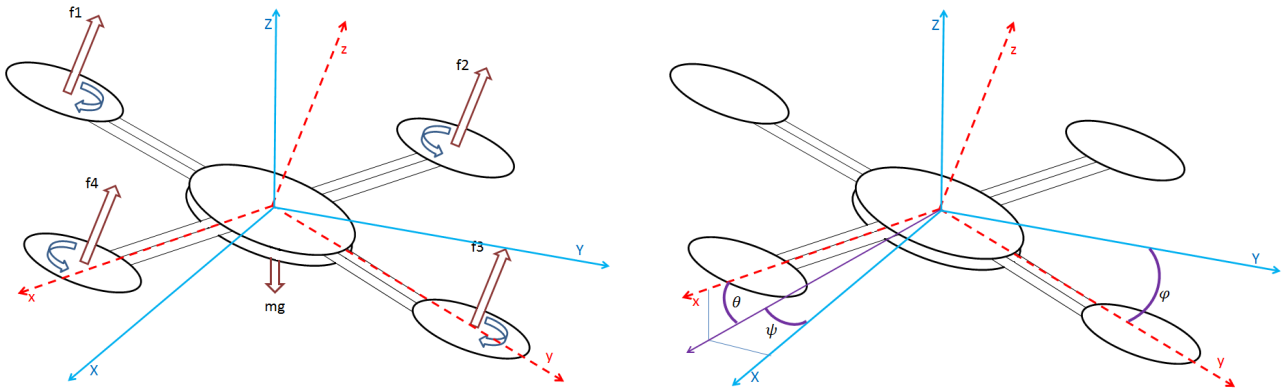

(a) Quadrotor freebody diagram

(b) Quadrotor co-ordinate frames

Figure 3.1: Freebody dynamics and Co-ordinate frames.

3.1.2 Coordinate Systems

In deriving the dynamics, a generalized set of co-ordinates are defined. These co-ordinate frames are summarized in Figure 3.1(b). The inertial position co-ordinates $[X, Y, Z]$ and the body-fixed co-ordinates $[x, y, z]$ are related by the rotation matrix $R \in SO(3)$ which can be represented using 3-2-1 Euler angles $\phi, \theta, \psi \in [0, 2\pi)$ such that,

$$\begin{bmatrix} X \\ Y \\ Z \end{bmatrix} = R \begin{bmatrix} x \\ y \\ z \end{bmatrix}, \tag{3.1}$$

where the rotation matrix R can be expressed in term of Euler angles as,

$$R = \begin{bmatrix} c\phi c\psi & -c\phi s\psi + s\phi s\theta c\psi & s\theta s\psi + c\phi s\theta c\psi \\ c\theta s\psi & c\phi c\psi + s\phi s\theta s\psi & -s\phi c\psi + c\phi s\theta s\psi \\ -s\theta & s\phi c\theta & c\phi c\theta \end{bmatrix} \tag{3.2}$$

where $c\phi = \cos\phi$ and $s\phi = \sin\phi$ for all three Euler angles.

Along with the 3-2-1 Euler angles, the angular rates in the body co-ordinates $(p\ q\ r)$, have a direct relationship to the euler angle rates as,

$$\begin{bmatrix} \dot{\phi} \\ \dot{\theta} \\ \dot{\psi} \end{bmatrix} = \begin{bmatrix} 1 & s\phi t\theta & c\phi t\theta \\ 0 & c\phi & -s\phi \\ 0 & \frac{s\phi}{c\theta} & \frac{c\phi}{c\theta} \end{bmatrix} \begin{bmatrix} p \\ q \\ r \end{bmatrix} \tag{3.3}$$

3.1.3 Equations of Motion

Using the Newton-Euler equations, the motion of the quadrotor can be described using

$$\begin{bmatrix} \ddot{x} \\ \ddot{y} \\ \ddot{z} \end{bmatrix} = \frac{1}{m}\vec{F} - \vec{\omega} \times \vec{v} \tag{3.4}$$

$$\begin{bmatrix} \dot{p} \\ \dot{q} \\ \dot{r} \end{bmatrix} = I^{-1}(\vec{M} - \vec{\omega} \times I\vec{\omega}) \tag{3.5}$$

where m is the mass of the quadrotor, $I \in \mathbb{R}^{3\times3}$ is the inertia matrix, $x_p = [X, Y, Z]^T$ denotes the position of the origin of the body fixed frame with respect to the inertial frame, $\omega = [p, q, r]^T$ denotes the standard angular body rates, and $\vec{F}$ and $\vec{M}$ represent the vector of external forces and moments, respectively.

3.1.4 Forces and Moments

The external forces in the inertial frame are given by

$$\vec{F} = mg\hat{e}_Z - u_t R\hat{e}_3 \tag{3.6}$$

where $\hat{e}_Z$ is the unit vector in the inertial Z axis, $\hat{e}_3$ is the unit vector in the body z axis and u_t is the total thrust generated by rotors as described in Section 3.1.5. The external moments in the body frame, $\vec{M}$ are given by,

$$\vec{M} = \vec{\tau} - G_a \tag{3.7}$$

where G_a represents the gyroscopic moments caused by the combined rotation of the four rotors and the vehicle body, and $\vec{\tau} = \begin{bmatrix} \tau_\phi & \tau_\theta & \tau_\psi \end{bmatrix}^T$ are the control torques generated by differences in the rotor speeds as described in Section 3.1.5. The vector G_a is given by

$$G_a = \sum_{i=1}^{4} J_p(\omega \times \hat{e}_3)(-1)^{i+1}\Omega_i \tag{3.8}$$

where J_p is the inertia of each rotor. In previous works, the J_p term is found to be small [4] and as such the gyroscopic moments are removed in the controller formulation. However, the rotor inertia terms are included in all quadrotor simulations and result in minor unmodeled nonlinearities to be rejected by the controllers.

In addition to the thrust dynamics, there are numerous aerodynamic and aeroelastic phenomenon that affect the flight of the quadrotor. These include [23],

- Thrust Variation: At high velocities and angles of attack, the rotor thrust and torque models of Eqn (3.11) is no longer valid. More complex models based on momentum theory are discussed in Hoffmann et al [23].
- Blade Flapping: In high speed flight, the advancing and retreating portions of the rotorblade generate unequal thrusts. This difference in thrusts causes the blade to 'flap' causing considerable disturbance in attitude control [33].
- Body Drag: The vehicle in high speed flight feels a considerable amount of drag. The drag is compounded when there are wind gusts creating random oscillating forces on the quadrotor.
- Ground Effects: When flying close to the ground (or during the landing stage), the downwash of the rotors creates an extra force buoying against the helicopters descent.

The methods above require extensive system identification and aerodynamic studies that are beyond the scope of this work. As such, the above sources of discrepancy in the dynamics are treated as disturbances that are especially prevalent in fast and/or high angle of attack flights. The drag forces created by wind gusts is included in the simulation studies shown in Section 3.3

3.1.5 Actuator Dynamics

The four rotors each generate forces f_i where $i \in 1, 2, 3, 4$ (shown in Figure 3.1(a)). The rotors are electronically controlled by Brushless DC motors. The torque (Q), rotor speed(ω), voltage(V) and current(I) dynamics can be summarized by [22],

$$Q = K_q I \tag{3.9}$$

$$V = R_a I + K_e \omega \tag{3.10}$$

where K_q, R_a and K_e are motor constants. The rotors generate thrust by changing the velocity of the air as it passes through the geometry of the rotorblade. As such, the thrust is highly dependent on blade geometry. However, when the freestream velocity (velocity of air relative to the vehicle) is approximately zero, the power generated by the rotors can be approximated by [27],

$$P = f v_h \tag{3.11}$$

$$v_h = \sqrt{\frac{f}{2\rho A}} \tag{3.12}$$

where, P is the power generated by the rotor, f is the thrust of the rotor, v_h is the change in velocity of the air through the rotor, ρ is the density of air and A is the area of the blade. In an effort to find a relationship between input voltage and rotor thrust, the power of the BLDC motors can be equated to the power of the rotors. This gives the relationship [22],

$$P = fv_h = VI = \frac{Q}{K_q}V \tag{3.13}$$

The reaction torque in the generated by each of the rotors, Q can be modeled as proportionally dependent on the thrust of the rotor, with the linear model defined by k_t [27]. Therefore,

$$\frac{Q}{K_q}V = \frac{k_t f}{K_q}V \tag{3.14}$$

Combining Eqn. (3.14) and Eqn. (3.13) gives the relationship [22],

$$f = \frac{2\rho A k_t^2}{K_q^2}V^2 \tag{3.15}$$

The constants above can be combined to a constant k_i which gives us the quadratic relationship for the rotor i,

$$f_i = k_i V^2 \tag{3.16}$$

Four of the thrusts above are combined to create a total body thrust u_t, as

$$u_t = f_1 + f_2 + f_3 + f_4$$

A difference in the rotor speeds creates a torque in the roll and pitch directions (τ_ϕ and τ_θ respectively), directly proportional to the distance of the motors to the center of gravity (l). The torque in the yaw direction (τ_ψ) is guided by an aerodynamic constant (c). These kinematic actuator relationships can be summarized as [16],

$$\begin{bmatrix} u_t \\ \tau_\phi \\ \tau_\theta \\ \tau_\psi \end{bmatrix} = \begin{bmatrix} 1 & 1 & 1 & 1 \\ -l & 0 & l & 0 \\ 0 & l & 0 & -l \\ c & -c & c & -c \end{bmatrix} \begin{bmatrix} f_1 \\ f_2 \\ f_3 \\ f_4 \end{bmatrix} \tag{3.17}$$

Note that the matrix in the above relationship has rank 4 (the matrix is invertible) and as such any set of *required* thrusts and torques can be resolved into forces to be generated

by each of the individual motors using Eqn (3.17). These forces can then be generated by the electronically controlled BLDC motors using the relationship in Eqn (3.16). The dynamics of the quadrotor with inputs $\begin{bmatrix} u_t & \tau_\phi & \tau_\theta & \tau_\psi \end{bmatrix}$ can be summarized as,

$$\begin{bmatrix} \ddot{x} \\ \ddot{y} \\ \ddot{z} \end{bmatrix} = \frac{1}{m}\vec{F} - \vec{\omega} \times \vec{v} \tag{3.18}$$

$$\begin{bmatrix} \dot{p} \\ \dot{q} \\ \dot{r} \end{bmatrix} = I^{-1}(\vec{M} - \vec{\omega} \times I\vec{\omega}) \tag{3.19}$$

where,

$$\vec{F} = mg\hat{e}_Z - u_t R\hat{e}_3 \tag{3.20}$$

$$\vec{M} = \begin{bmatrix} \tau_\phi & \tau_\theta & \tau_\psi \end{bmatrix}^T \tag{3.21}$$

3.2 Control Techniques

3.2.1 Linear Quadratic Regulation for Quadrotor Helicopters

Most previous works in LQR control of quadrotors have considered a nested control structure, where an inner loop controls the roll, pitch and yaw of the vehicle [5]. An outer loop to control the position of the vehicle is then designed assuming the orientation angles can be achieved with negligible delay. However, for this work, this decoupling is removed in favour of a full state controller. The design is then prioritized for the states of most importance for most UAV systems, position (x, y, z) and yaw (ψ). The full state controller uses the dynamics as described in Eqn. (3.4) and (3.5). These dynamics are linearized around hover using the state $x = \begin{bmatrix} X & Y & Z & \dot{X} & \dot{Y} & \dot{Z} & \phi & \theta & \psi & p & q & r \end{bmatrix}$ and input $u = [u_t, \tau_\phi, \tau_\theta, \tau_\psi]$. The state and inputs at hover would be $x_0 = 0$ and $u_0 = \begin{bmatrix} mg & 0 & 0 & 0 \end{bmatrix}$. With this, the linearized system can be represented as,

$$\dot{x} = Ax + Bu \tag{3.22}$$

where,

$$A(x, u) = \frac{\partial \dot{x}}{\partial x} \tag{3.23}$$

$$B(x, u) = \frac{\partial \dot{x}}{\partial u} \tag{3.24}$$

where the function $\dot{x}$ is as described in Eqn. (3.4) and (3.5). The matrices A and B can then be acquired by substituting for the linearized states and inputs, $A = A_t(x_0, u_0)$ and $B = B_t(x_0, u_0)$.

Given the linearization in Eqn (3.22), the following quadratic cost function,

$$J = \int x^T Q x + u^T R u \tag{3.25}$$

is used, where Q and R are the relative scaling matrices for the state and input costs respectively. This cost function can be optimized with the control input [38],

$$u(t) = -K_c x(t) \tag{3.26}$$

Here,

$$K_c = R^{-1} B^T P$$

where P obeys the Ricatti Equation,

$$-PA - A^T P + PBR^{-1}B^T P - Q = \dot{P} \tag{3.27}$$

In the steady state case with infinite horizon optimization, Eqn (3.27) can be solved with $\dot{P} = 0$. A derivation for the optimization problem can be found in various works, [38, 5]. The LQR problem is solved for the system and linearization described in Eqn (3.22) with Q and R matrices that contain the relative importance of tracking each state. In this case all the states and inputs are given equal importance (i.e. the Q and R matrices are identity). However, this could be modifed if certain states have a higher accuracy requirement. Using these identiy Q and R matrices the Ricatti equation can then be solved for a static gain K_c that is calculated before flight. This static gain is used in a simulation of the dynamics and controller. Figure 3.2 and Figure 3.3 shows the position control results of a unit step command given to the quadrotor. In Figure 3.2 it is clear that the quadrotor is able to successfully track the required position command using the LQR controller and settles onto the required position in less than 4 seconds. The response of the system when commanded to track more complex trajectories can be found in Section 3.3.

3.2.2 Feedback Linearization for Quadrotor Helicopters

Feedback Linearization (also referred to as Dynamic Inversion) is a popular method for control for nonlinear systems. A full description of this methodology can be found in current literature [25]. A summary is presented here along with a derivation for quadrotor dynamics.

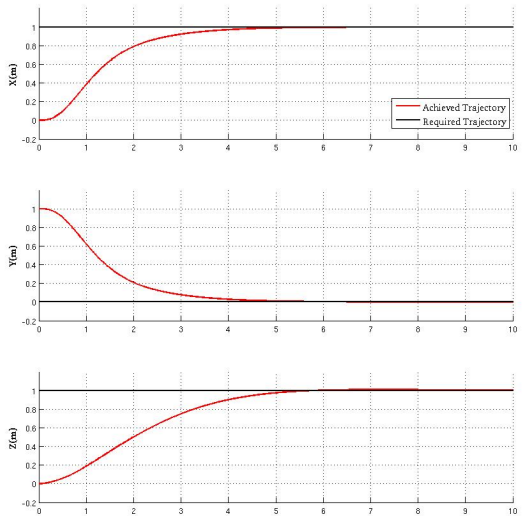

Figure 3.2: Position response of the LQR controller to a step input

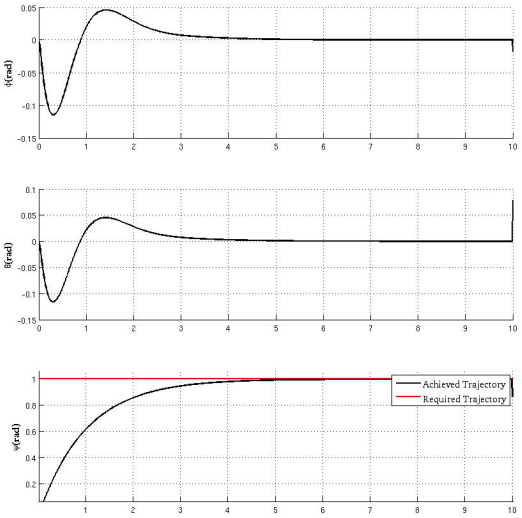

Figure 3.3: Attitude Response of the LQR controller to a step input

Feedback Linearization Controller Formulation

Given a state x and output y and dynamics that can be expressed in control affine form,

$$\dot{x} = f(x) + g(x)u \tag{3.28}$$
$$y = h(x) \tag{3.29}$$

where f, g and h are sufficiently smooth and with $x \in \mathbb{R}^n$. Consider for now, that this is a single-input, single-output system, i.e. $u, y \in \mathbb{R}^1$. The derivative of the output y can be expressed as [25],

$$\dot{y} = \frac{\partial h}{\partial x}[f(x) + g(x)u \tag{3.30}$$

The derivative of h along the trajectory of the state $\dot{x}$ is known as the *Lie Derivative* denoted as,

$$\frac{\partial h}{\partial x}[f(x) + g(x)u = L_f h(x) + L_g h(x)u \tag{3.31}$$

If on the first derivative $L_g h(x) = 0$ as in,

$$\dot{y} = y^{(1)} = L_f h(x) \tag{3.32}$$

note that the output y remains independent of input u. However, subsequent higher order derivatives can be taken such that,

$$y^{(2)} = L_f^2 h(x) + L_g L_f h(x)u \tag{3.33}$$
$$y^{(3)} = L_f^3 h(x) + L_g L_f^2 h(x)u \tag{3.34}$$
$$y^{(i)} = L_f^i h(x) + L_g L_f^{i-1} h(x)u \tag{3.35}$$

and if for a certain i, $L_g L_f^j h(x)u \neq 0$, then the equation

$$y^{(i)} = L_f^i h(x) + L_g L_f^{i-1} h(x)u \tag{3.36}$$

can be linearized with full state feedback by,

$$u = \frac{1}{L_g L_f^{i-1} h(x)}(-L_f^i h(x) + v) \tag{3.37}$$

in the region that the inverse $\frac{1}{L_g L_f^{i-1} h(x)}$ exists. In this region the feedback linearized model becomes,

$$y^{(i)} = v \tag{3.38}$$

The value i is defined to be the *relative degree* of the system. The resulting linear dynamic system defined in Eqn (3.38) can be stabilized by most linear control techniques and consists of a set of i-1 integrators to the required output y. Moreover, with this linearization and assuming such a relative degree exists a linear controller can be designed such that the overall system can be proven to be exponentially stable [25]. Finally, if $u \in \mathbb{R}e^p$ and $y \in \mathbb{R}e^m$ in Eqn (3.28) then for the feedback linearization to be possible the matrix $L_g L_f^{i-1} h(x)$ must be square and full rank. Moreover the sum of the relative degrees of all the inputs must equal the number of states in x. If the sum of the relative degrees is not equal to the number of states then there are states that are not directly controllable through the inputs. These extra states are called *zero dynamics* and must be proven to be stable externally.

Feedback Linearization Quadrotor Dynamics

The quadrotor helicopter has six output states $y = (X, Y, Z, \phi, \theta, \psi)$. The vehicle has four inputs as shown in Eqn (3.17). Das et al. [16] shows that the relative degree is not equal to the number of states to be controlled. There are two states that are left uncontrollable and must be proven stable. A solution suggested by previous works [26, 3, 1] uses *dynamic extension* as a method to add virtual inputs to control these zero dynamics. However, for the virtual inputs to affect the zero dynamics, more derivatives must be taken as shown in Eqn (3.33). In implementation this would imply the system would need to 3rd or 4th order derivatives of the orientation and/or position states. In most quadrotor platforms, these states are measured using noisy MEMS sensors, GPS recievers or indoor localization methods. Taking derivatives of these measurements leads to amplification of measurement noise, which can cause significant chatter in the system. This factor is confirmed by the feedback linearization methodology implemented on quadrotors by Shastry et al. [26]. Another solution to this problem is to decompose the problem into two distinct control loops. The two control loops comprise of an inner loop that controls the height and attitude of the system, and an outer loop that controls the position. This solution was first suggested by Das et al. [16]. This controller is used as a baseline for the feedback linearization controller in this work.

First, consider the *inner loop* of the quadrotor system as the height and attitude(i.e $x_q = \begin{bmatrix} Z & \phi & \theta & \psi \end{bmatrix}^T$). For this system, the traditional feedback linearization methodology can

be applied here with the output equation $y = x_q$ as per Eqn (3.28). Picking this inner loop as the output equation, the first derivative would lead to $\dot{y} = \begin{bmatrix} \dot{Z} & \dot{\phi} & \dot{\theta} & \dot{\psi} \end{bmatrix}^T$. Note here that the control input dependent term $L_g h(x)$ is zero. Taking the second derivative of the state makes the dynamics summarized in Eqns (3.4) and (3.5) appear as,

$$\ddot{x^q} = \begin{bmatrix} \ddot{Z} \\ \ddot{\phi} \\ \ddot{\theta} \\ \ddot{\psi} \end{bmatrix} = A_d + B_d u_d \tag{3.39}$$

where,

$$A_d = \begin{bmatrix} -g \\ \dot{\theta}\dot{\psi}\frac{I_y - I_z}{I_x} \\ \dot{\phi}\dot{\psi}\frac{I_z - I_x}{I_y} \\ \dot{\phi}\dot{\theta}\frac{I_x - I_y}{I_z} \end{bmatrix} \tag{3.40}$$

$$B_d = \begin{bmatrix} -\frac{1}{m}c_\theta c_\phi & 0 & 0 & 0 \\ 0 & \frac{1}{I_x} & 0 & 0 \\ 0 & 0 & \frac{1}{I_y} & 0 \\ 0 & 0 & 0 & \frac{1}{I_z} \end{bmatrix} \tag{3.41}$$

$$u_d = \begin{bmatrix} u \\ \tau_\phi \\ \tau_\theta \\ \tau_\psi \end{bmatrix} \tag{3.42}$$

Here a simplification is made by setting $\begin{bmatrix} \phi & \theta & \psi \end{bmatrix} = \begin{bmatrix} p & q & r \end{bmatrix}$. This is contrary to the dynamics described in Eqn. (3.3). This assumption simplifies the derivation of the feedback linearization controller as the derivatives of the dynamics in Eqn. (3.3) are highly complex. The assumption holds true for smaller angles of movement. However, the nonlinear structure is still superior to a complete linear simplification because the nonlinear quadrotor dynamics shown in Eqn. (3.39) account for fast angular movements closer to hover. Moreover, at extreme angles the more complex aerodynamic phenomenon described in Section 3.1.4 may become more dominant than the trigonometric nonlinearities described in (3.3).

Based on the dynamics described in (3.39), the control input can be selected as per Eqn (3.37) to be,

$$u_d = B_d^{-1}(-A_d + \ddot{x}^{q*}) = M^q(x^q)\ddot{x^{q*}} + C^q(x^q, \dot{x^q}) \tag{3.43}$$

where,

$$M^q(x^q) = \begin{bmatrix} -\frac{m}{c_\theta c_\phi} & 0 & 0 & 0 \\ 0 & I_x & 0 & 0 \\ 0 & 0 & I_y & 0 \\ 0 & 0 & 0 & I_z \end{bmatrix} \tag{3.44}$$

$$C^q(x^q, \dot{x}^q) = \begin{bmatrix} \frac{g}{c_\theta c_\phi} \\ \dot{\theta}\dot{\psi}(I_z - I_y) \\ \dot{\phi}\dot{\psi}(I_x - I_z) \\ \dot{\phi}\dot{\theta}(I_y - I_x) \end{bmatrix} \tag{3.45}$$

Note that $C^q(x^q, \dot{x}^q)$ exists for the region $-90^\circ < \theta, \phi < 90^\circ$. Furthermore, the remaining linear dynamics after feedback linearization are an integrator chain, $\ddot{x}^q = \ddot{x}^{q*}$, which can be controlled by the linear controller,

$$\ddot{x}^{q*} = \ddot{x}^q_d - k_v(\dot{x}^q - \dot{x}^q_d) - k_p(x^q - x^q_d) \tag{3.46}$$

where, $\ddot{x}_d$ is the desired acceleration of the inner loop, x^q_d and $\dot{x}^q_d$ are the desired trajectories for the state and its velocities. Finally, $k_v > 0$ and $k_p > 0$ are tunable gains that can be used to place the poles of the subsequent feedback linearized dynamics on the left hand side plane. Using the controller described in Eqn (3.43) and Eqn. (3.46) the attitude of the controller can be stabilized and arbitrarily commanded.

The controller in Eqn (3.46) and its related feedback linearization method stabilizes the attitude dynamics of the system. However, the position dynamics (internal states) still remain unstable. These dynamics as per Equation (3.4) are,

$$\ddot{x} = \frac{-u}{m}\sin\theta \tag{3.47}$$

$$\ddot{y} = \frac{u}{m}\cos\theta\sin\phi \tag{3.48}$$

Das [16] suggests a method to control these dynamics by controlling the desired roll (θ_d) and pitch(ϕ_d) angle shown in Eqn. (3.46) as part of x_d. As before there is a chain of two integrators to get to the desired position variables (x, y). Therefore, The same linear controller used in the inner loop control is applied to stabilize the outer loop dynamics,

$$\theta_d = -\frac{m}{u}[\ddot{x_d} + k_{11}(\dot{x_d} - \dot{x}) + k_{12}(x_d - x)] \tag{3.49}$$

$$\phi_d = \frac{m}{u}[\ddot{y_d} + k_{11}(\dot{y_d} - \dot{y}) + k_{12}(y_d - y)] \tag{3.50}$$

where (x_d, y_d) is the required position trajectory for the vehicle along with its derivatives and k_{ii} are tunable gains that can be used to place the poles of the position dynamics of the system on the left hand plane. This position controller along with the feedback linearized inner loop has been demonstrated to be stable [16].

Figure 3.4 shows the result of the feedback linearization controller when given a position control command. Figure 3.5 shows the resultant orientation results. The controller is shown to be stable and gives results similar to that of the LQR controller in Section 3.2.1. Comparitive results of the various controllers to different reference trajectories can be found in Section 3.3.

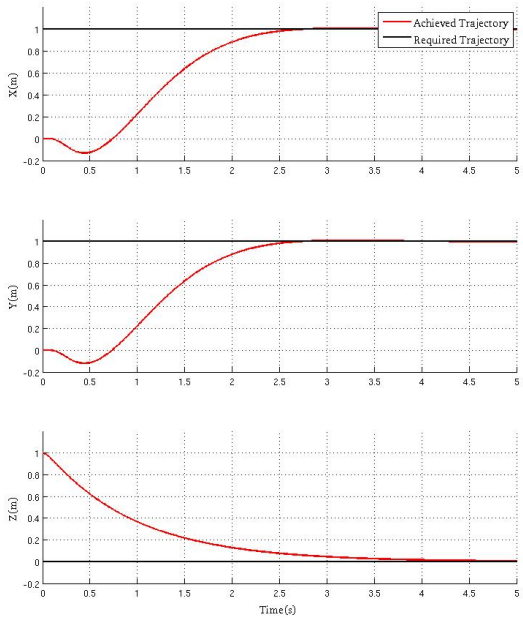

Figure 3.4: Position response of the Feedback Linearization controller to a step input

3.2.3 Adaptive Feedback Linearization for Quadrotor Attitude Control

The primary drawback of the feedback linearization technique is that it assumes accurate knowledge of the nonlinear model to guarantee stability, and unmodeled nonlinearities

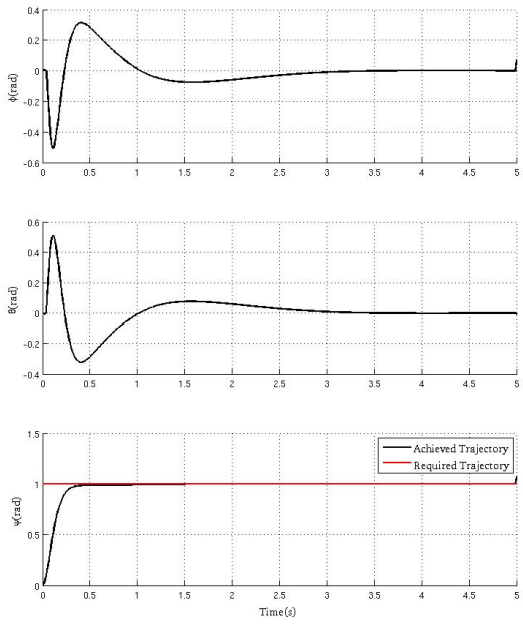

Figure 3.5: Attitude Response of the Feedback Linearization controller to a step input

frequently limit the applicability of feedback linearization in practice [26]. A major source of errors in the models can be attributed to inaccuracies in the parameters that drive the dynamics. In the case of the quadrotor, these parameters include the mass m and the quadrotor inertia (I_x, I_y, I_z) as part of the inertia matrix in Eqn. (3.5). These parameters are not always known to adequate accuracy, and may even change during flight. This can cause significant error in the feedback linearization and may also cause instabilities in the system. Adaptive control methods have been proposed as a method to adapt parameters to strengthen control algoritms sensitive to accuracies therein. As such, an adaptive law around the feedback linearization method is derived here. This method was first suggested by [15] for mechanical manipulators, however a summary of the derivation and its evaluation for quadrotor helicopters is presented here.

Adaptive Controller Formulation

Given a state x and input torques τ, a large class of mechanical systems (including the quadrotor helicopter) can be expressed in the form:

$$u = M(x,p)\ddot{x} + C(x,\dot{x},p) \tag{3.51}$$

where the nonlinear functions M and C describe the dynamics of the system and are assumed to be linear with respect to the parameters, p. The above dynamics can be controlled by the feedback linearizing controller,

$$u = M(x,p)\ddot{x}^* + C(x,\dot{x},p) \tag{3.52}$$

where we choose,

$$\ddot{x}^* = \ddot{x}_d + k_v\dot{E} + k_pE \tag{3.53}$$

where, $\ddot{x_d}$ are the desired state accelerations, $\dot{E}$ and E are the state error velocities and positions defined as $E = x_d - x$ and $\dot{E} = \dot{x_d} - \dot{x}$

The gains k_v and k_p can be picked to place the poles of the linearized closed loop dynamics in the left hand plane. However, in Eqn (3.51) if the functions M and C are unknown due to parameter error, they can be estimated with $\hat{M}$ and $\hat{C}$ which are linear with respect to the unknown parameters $\hat{p}$. Therefore, the control becomes,

$$u = \hat{M}(x,\hat{p})\ddot{x}^* + \hat{C}(x,\dot{x},\hat{p}) \tag{3.54}$$

A parameter adaptation law can now be derived by first re-defining the system dynamics in parameter error terms. First define,

$$\begin{aligned} \tilde{M} &= M - \hat{M} && (3.55) \\ \tilde{C} &= C - \hat{C} && (3.56) \\ \Phi &= p - \hat{p} \end{aligned}$$

which are the errors in the two matrices M and C and the parameter error, Φ. Inserting the control law in Eqn (3.54) into the dynamics in Eqn (3.51) and subtracting $\hat{M}(x, \hat{p})\ddot{x}$ from both sides yields,

$$\tilde{M}(x, \Phi)\ddot{x} + \tilde{C}(x, \dot{x}, \Phi) = \hat{M}(x, \hat{p})(\ddot{E} + k_v\dot{E} + k_pE) \tag{3.57}$$

which leads to the following equation for the error dynamics,

$$\ddot{E} + k_v\dot{E} + k_pE = \hat{M}^{-1}(\tilde{M}(x, \Phi)\ddot{x} + \tilde{C}(x, \dot{x}, \Phi)) \tag{3.58}$$

The matrices for the dynamics (Eqn (3.51)) are linear with respect to the parameters p. Therefore, the dynamics in error terms can be rewritten as,

$$\tilde{M}(x, \Phi)\ddot{x} + \tilde{C}(x, \dot{x}, \Phi) = W(x, \dot{x}, \ddot{x})\Phi \tag{3.59}$$

where, W is a nonlinear matrix that captures the dependence of the error dynamics on the parameters. Therefore, the system dynamics from Eqn. (3.58) can be written as,

$$\ddot{E} + k_v\dot{E} + k_pE = \hat{M}(x, \hat{p})^{-1}W(x, \dot{x}, \ddot{x})\Phi \tag{3.60}$$

Using the above equations, consider the system with the state $x_e = \begin{bmatrix} E & \dot{E} \end{bmatrix}^T$ which would have the dynamics,

$$\dot{x}_e = Ax_e + B\hat{M}^{-1}W\Phi \tag{3.61}$$

where,

$$A = \begin{bmatrix} 0 & I \\ k_p & k_v \end{bmatrix}$$

$$B = \begin{bmatrix} 0 \\ I \end{bmatrix}$$

With the above system, consider the output equation

$$E_1 = Cx_e \tag{3.62}$$

with $C = \begin{bmatrix} \Psi & I \end{bmatrix}$ and Ψ is a tunable gain. The variable E_1 is effectively a filtered output error signal. For the above system, consider the Lyapunov Function

$$V = x_e^T P x_e + \Phi^T \Gamma^{-1} \Phi \tag{3.63}$$

where $\Gamma > 0$ is the adaptation gain and $P > 0$. The Kalman-Yakubovich-Popov Lemma guarantees that if,

- A is Hurwitz (choice of k_v and k_p will ensure of this) and,
- (A, B) is controllable,

then there exists a matrix $Q > 0$ such that,

$$A^T P + PA = -Q \tag{3.64}$$

$$PB = C^T \tag{3.65}$$

Using this, the derivative of the signal in Eqn (3.63) along the trajectory of the system can be shown to be [15],

$$\dot{V} = -x_e^T Q x_e + 2\Phi^T (W^T \hat{M}^{-1} E_1 + \Gamma^{-1} \dot{\Phi}) \tag{3.66}$$

Choosing the adaptation law,

$$\dot{\Phi} = -\Gamma W^T \hat{M}^{-1} E_1$$

the energy function in Eqn (3.66) becomes,

$$\dot{V} = -x_e^T Q x_e$$

which is negative semidefinite for all $Q > 0$ and $x_e \in \mathbb{R}^n$. Note here that, $\Phi = p - \hat{p}$ and $\dot{\Phi} = -\dot{\hat{p}}$. Therefore, the resultant parameter adaptation law would be,

$$\dot{\hat{p}} = \Gamma W^T \hat{M}^{-1} E_1 \tag{3.67}$$

According to Lyapunov theory [25], the adaptation law given in Eqn (3.67) used with the control law in Eqn (3.54) ensures bounded stability around the error surface defined in Eqn (3.62).

Adaptive Controller for Quadrotor Dynamics

The quadrotor helicopter dynamics presented in Section 3.1 have four critical parameters, as mentioned before. These parameters can be arranged in the parameter vector as,

$$p^q = \begin{bmatrix} p_1^q \\ p_2^q \\ p_3^q \\ p_4^q \end{bmatrix} = \begin{bmatrix} m \\ I_x \\ I_y \\ I_z \end{bmatrix} \tag{3.68}$$

Note that this choice of p ensures the system in Eqn (3.43) is linear in the parameters.

In Section 3.2.2, a feedback linearizing controller was designed for the inner loop for $x^q = \begin{bmatrix} Z & \phi & \theta & \psi \end{bmatrix}^T$. This feedback linearizing controller can be re-interpreted to include the parameter vector (p^q) as,

$$u = M^q(x^q, p^q)\ddot{x^q}^* + C^q(x^q, \dot{x^q}, p^q) \tag{3.69}$$

where,

$$u^q = \begin{bmatrix} u_t^q \\ \tau_\phi^q \\ \tau_\theta^q \\ \tau_\psi^q \end{bmatrix} \tag{3.70}$$

$$M^q(x, p^q) = \begin{bmatrix} -\frac{m}{c_\theta c_\phi} & 0 & 0 & 0 \\ 0 & I_x & 0 & 0 \\ 0 & 0 & I_y & 0 \\ 0 & 0 & 0 & I_z \end{bmatrix} \tag{3.71}$$

$$C^q(x^q, \dot{x^q}, p^q) = \begin{bmatrix} \frac{g}{c_\theta c_\phi} \\ \dot{\theta}\dot{\psi}(I_z - I_y) \\ \dot{\phi}\dot{\psi}(I_x - I_z) \\ \dot{\phi}\dot{\theta}(I_y - I_x) \end{bmatrix} \tag{3.72}$$

Finally, as per the variable $W(x, \dot{x}, \ddot{x})$ in Eqn (3.59), one can define,

$$W(\ddot{x^q}, \dot{x^q}, x^q) = \begin{bmatrix} \frac{-\ddot{Z}+g}{c_\theta c_\phi} & 0 & 0 & 0 \\ 0 & \ddot{\phi} & \dot{\theta}\dot{\psi} & -\dot{\theta}\dot{\psi} \\ 0 & -\dot{\phi}\dot{\psi} & \ddot{\theta} & \dot{\phi}\dot{\psi} \\ 0 & \dot{\theta}\dot{\phi} & -\dot{\theta}\dot{\phi} & \ddot{\psi} \end{bmatrix} \tag{3.73}$$

Using the definition in Eqn (3.73), the parameter adaptation law for the quadrotor vehicle would be,

$$\dot{\hat{p}}^q = -\Gamma W^T \hat{M}^{q^{-1}} E_1 \tag{3.74}$$

where adaptation gain Γ and tracking error surface E_1 are defined in Eqn (3.63) and Eqn.(3.62), respectively. This parameter adaptation law, along with the control law in Eqn (3.69) can now be use to stabilize the quadrotor dynamics with unknown inertia and mass parameters. Note here that the parameter adaptation law is driven by trajectory errors $(E, \dot{E})$ and not plant errors. Therefore, the overall goal for this controller is to reduce tracking error and not necessarily to achieve consistent and universally correct inertia and mass terms. If the input trajectories are sufficiently rich (contain an adequate number of frequencies), then the parameters may become correct and consistent. However, this is not a requirement for safe and accurate flight.

Figure 3.6 shows the result of a simulated quadrotor flight using the adaptive feedback linearization controller. The quadrotor is commanded to follow a sinusoidal trajectory using the feedback linearization method, however the parameters used for the feedback linearization are initialized to have over 40% error. Figures 3.6 and 3.7 show that the adaptive controller is able to stabilize the dynamics to the required path and follow an aggressive trajectory. Moreover, Figure 3.8 shows the result of the parameter adaptation. In the trajectory shown in Figure 3.6, the trajectory is sufficiently rich so that the parameters converge to the correct parameters.

3.3 Comparitive Results

In an effort to evaluate the strengths of each controller, the simulation results are directly compared under various circumstances. First, the linear (LQR) and nonlinear feedback linearization controllers are compared when experiencing aggressive input trajectories. The performance of the controllers is shown in Figure 3.9 and Figure 3.10 for the position and orientation response respectively. It is clear from these figures that the LQR controller is unable to provide adequate tracking for aggressive trajectories. This is primarily due to the fact that the LQR controller is designed around the linear hover point. An aggressive trajectory, as shown in Figure 3.10, pushes the vehicle dynamics far outside this linearization point rendering the linear controller ineffective.

In an effort to show the specific advantages of adaptation, the simulation is subjected to three different flight scenarios,

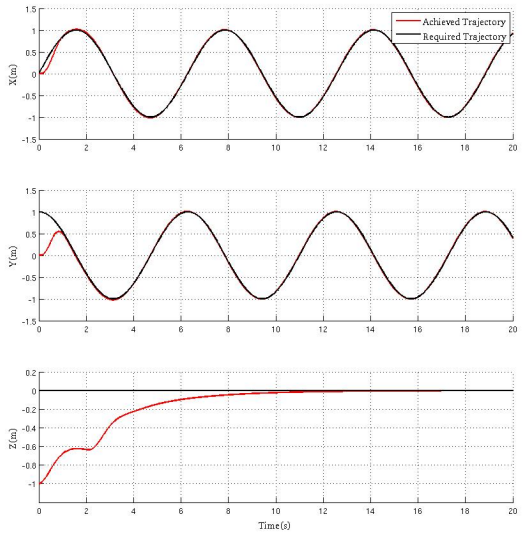

Figure 3.6: Position response of the Adaptive Feedback Linearization controller to a step input

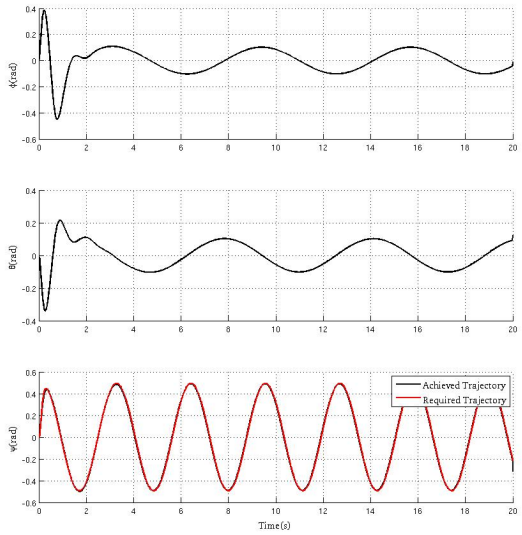

Figure 3.7: Attitude Response of the Adaptive Feedback Linearization controller to a step input

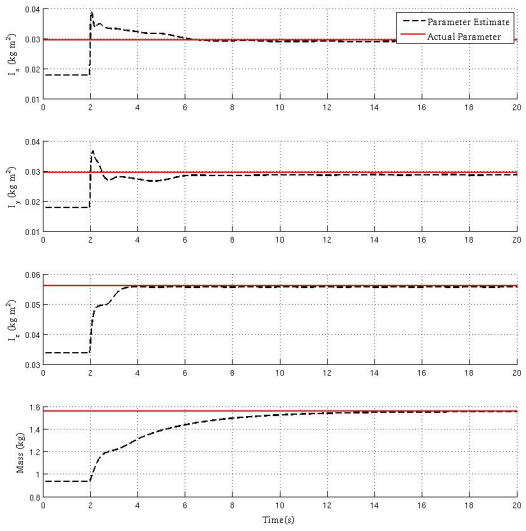

Figure 3.8: Parameter adaptation for Adaptive Controller with upto 40% parameter error

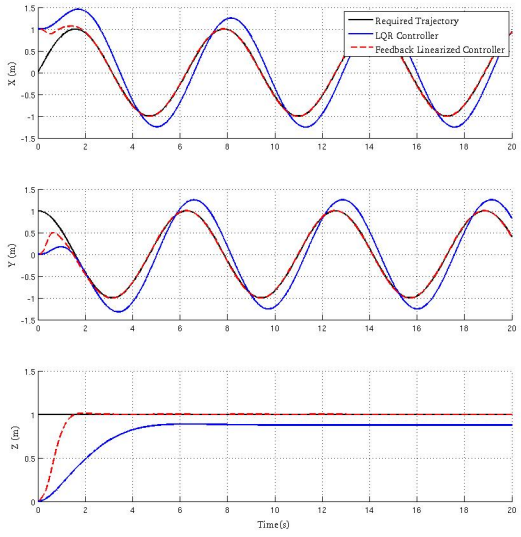

Figure 3.9: Position Tracking with LQR and Feedback Linearization Controllers

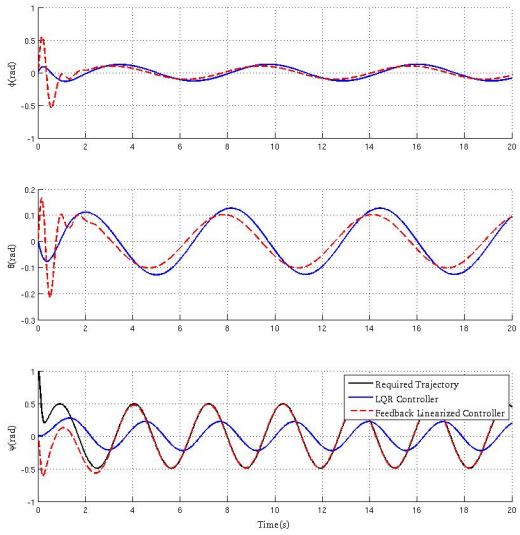

Figure 3.10: Orientation Tracking with LQR and Feedback Linearization Controllers

- Flight with incorrect model parameters (up to 40% error) with and without adaptation.
- Flight with random parameter changes during flight, due to payload changes, physical breakage etc.
- Flight with external disturbances and incorrect model parameters (up to 30% error).

Figures 3.11, 3.12 and 3.13 present the results of a simulated flight using the adaptive feedback linearization controller with up to 40% error in initial flight parameter estimates.

It is clear from the position tracking results in Figure 3.11 that there is a substantial improvement in tracking due to the adaptation. The parameters used for feedback linearization are close enough to their respective correct values to allow the linear controller in Eqn (3.53) to keep the flight stable. However, after the adaptation is turned on, the controller shows improved tracking results. As described in Section 3.2.3, the adaptation is driven by trajectory errors and not plant errors. Therefore, the parameters are not guaranteed to converge to the universally correct parameters. Convergence will depend on the richness and complexity of the required input trajectory. As seen in Figure 3.13, with

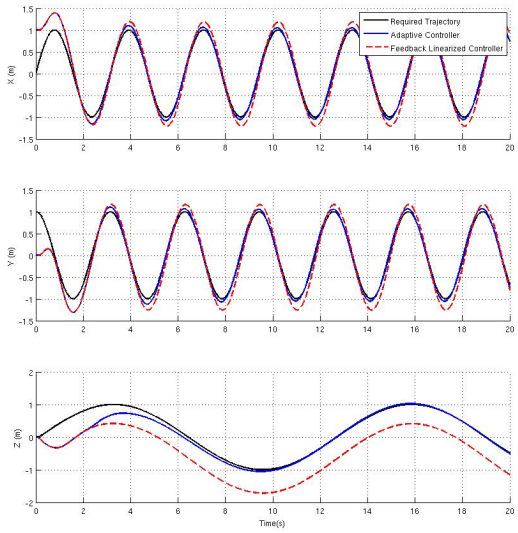

Figure 3.11: Position Tracking with and without adaptive control

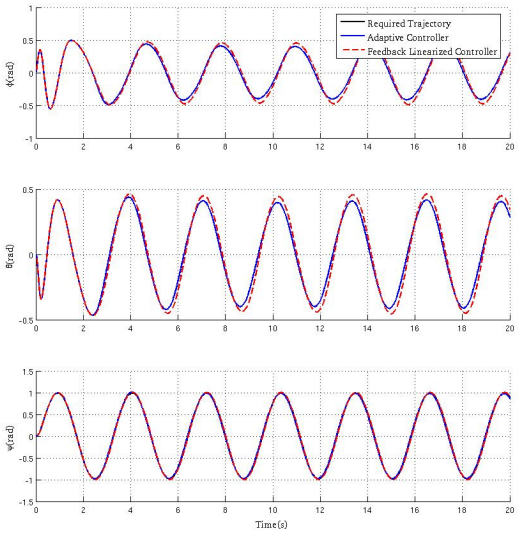

Figure 3.12: Quadrotor Orientation with and without adaptive control

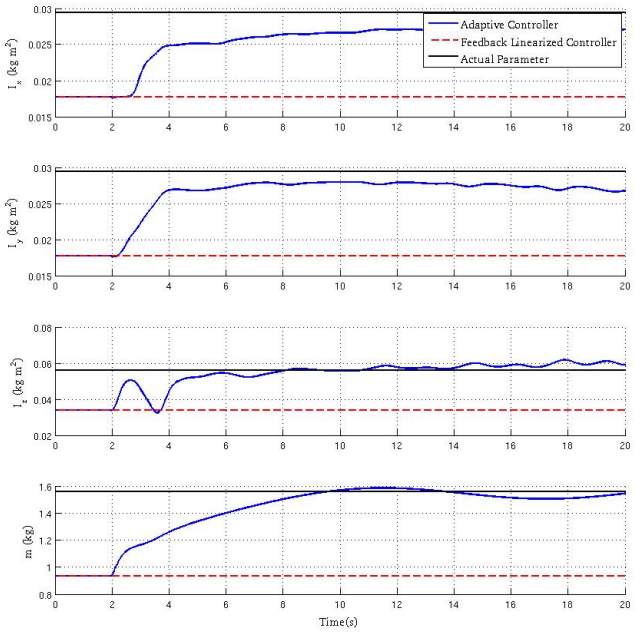

Figure 3.13: Parameter adaptation with and without Adaptive Control

the trajectory shown in Figure 3.11 the parameters do converge to their respective correct values.

Parameter changes during the flight of a helicopter can significantly deteriorate and even destabilize a controller. During quadrotor flight, the most common parameter change is a change in mass due to changes in payload. This scenario is simulated in Figure 3.3. Figure 3.3 shows that when the mass of the vehicle changes (after about 10 seconds of flight), the feedback linearized controller is unable to accurately control the vehicle. The error in tracking could be reduced by drastically increasing the linearized gains, however the incorrect feedback linearization will always cause significant steady state error. Simply adding an integrator may also reduce the tracking error. However, this will add extra dynamics to the controller and make it difficult to tune. Moreover, an integrator is not as effective in improving the *transient dynamics* of the vehicle. In general, if there are changes in vehicle parameters during flight, a feedback linearized or PID controller will always need to be re-tuned for the performance of the controller to stay the same. The adaptive controller is able to maintain the performance by adapting the estimate of mass *online*. This allows the quadrotor vehicle to safely change plant parameters without the risk of degraded controller performance or destabilization.

Finally, most sUAV's are sensitive to various environmental effects such as wind gusts outdoors or turbulent air when flying indoors due to the airflow created by rotors. The scenario with these external effects is simulated using a variant of the Dryden wind gust model as in the case of the coaxial helicopter before. The results of such a flight are presented in Figure 3.15 and Figure 3.16. Figure 3.17 presents the parameter adaptation of the quadrotor vehicle in these conditions.

Figure 3.15 result shows that under gusty wind conditions the flight under regular feedback linearization has significantly deteriorated. The simulated conditions contain a constant bias in the form of a constant force as is common in windy conditions. This constant bias also causes a constant position tracking error in addition to the significant ringing in the orientation tracking of the vehicle. In the case of the adaptive controller, the vehicle adapts the parameters so as to minimally suppress the ringing in orientation. Moreover, the parameter adaptation significantly reduces the tracking error caused by the combination of windy conditions and parameter error. In the case of altitude tracking the estimate of the parameter is moved to its actual value ($1.5kg$) to enable accurate tracking of the vehicle, the effect of the wind is minimal. However, in the case of x, y position tracking, the inertia parameters that primarily enable effective attitude tracking are increased to be significantly above the actual value. The increase in parameters allows the quadrotor vehicle to assume that the quadrotor is heavier (in inertia terms) than its actual parameters. Due to this adaptation, the feedback linearization controller responds

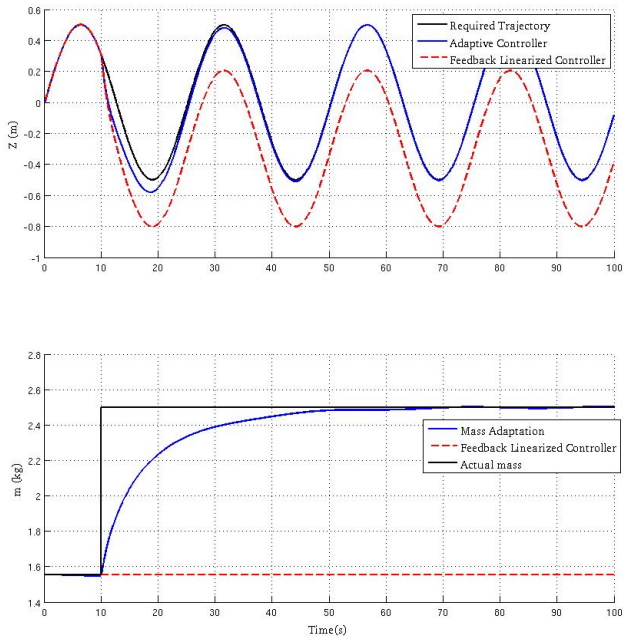

Figure 3.14: Quadrotor flight with parameter (mass) changes mid-flight

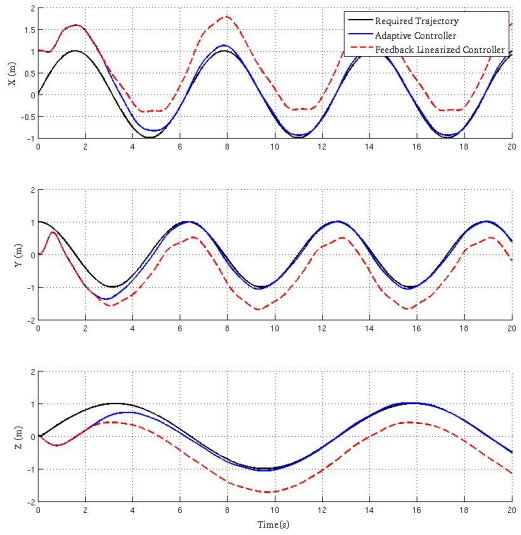

Figure 3.15: Position Tracking with and without adaptive control

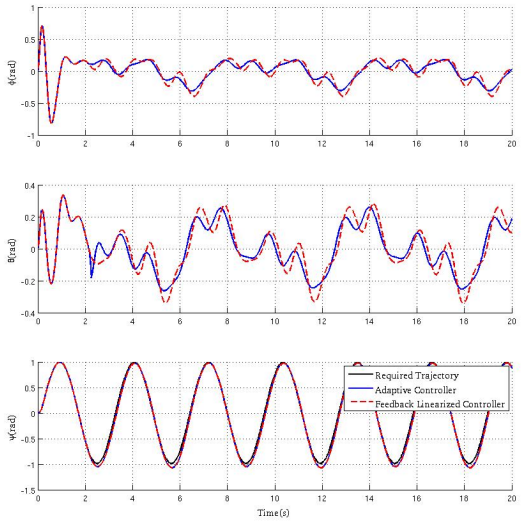

Figure 3.16: Quadrotor Orientation with and without adaptive control

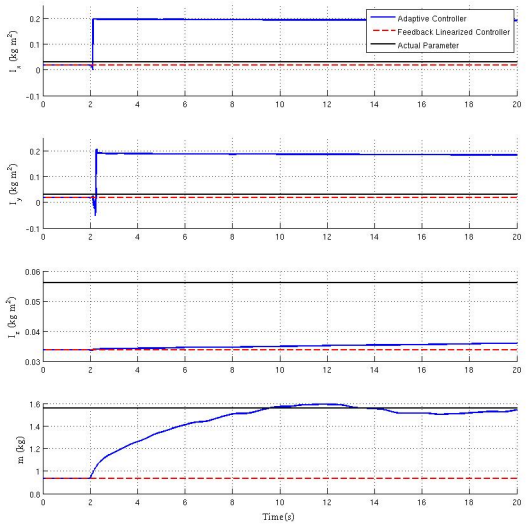

Figure 3.17: Parameter adaptation with and without Adaptive Control under windy conditions

by using more input torque to effectively overcome the effects of the wind gusts. The increased input torque results in accurate tracking of the required attitude trajectory and the resultant position tracking as shown in Figure 3.15.

Chapter 4

Experimental Flight Testbed and Results

4.1 Autopilot Platform

In an effort to create a testbed of helicopter platforms for the testing of the controllers presented in Sections 2 and 3, a versatile and customizable autopilot testbed was required. Autopilot systems are most commonly designed for specific aerial platforms, however for sUAV systems it is possible to build a single autopilot system that is able to serve the needs of various flight systems. Such an autopilot system was required in this work to be installed on Quadrotor Helicopters, Coaxial Helicopters and potentially other flight configurations. This autopilot system has three main requirements,

- The platform has to be small, compact and lightweight so that it could be mounted on and lifted by most sUAV platforms.
- The platform must employ high quality MEMS sensor systems to provide the best sensor measurements to aid in the control
- The system needs substantial computational power and high bandwidth communication capabilities to allow for the implementation of the various controllers suggested and all the supporting estimation and sensor systems.
- The system needs to have a flexible software architecture to allow for future expansion into more complex autonomy software.

A range of publicly available, open source and/or commercial solutions were considered. A few of the most popular autopilot systems are shown in Figure 4.1.

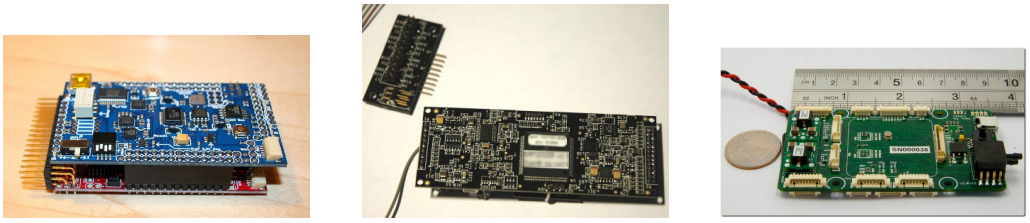

(a) Ardupilot (b) Micropilot (c) Paparazzi Lisa

Figure 4.1: Popular sUAV Autopilot Systems

The Ardupilot platform shown in Figure 4.1(a) is one of the most popular open-source autopilot platforms used. It is compact and has been installed on a large number of rotor and fixed wing aircrafts. However, the Ardupilot is based on a low-power ($< 16Mhz$) ATMEGA microcontroller framework that will not be able to the support the heavy computation required for the controllers and its related estimation algorithms. The Micropilot shown in Figure 4.1(b) is a popular commercial autopilot solution especially for rotorcrafts, however it does not allow for software architecture customization and is therefore inappropriate for controller studies. Finally, the Paparazzi platform shown in Figure 4.1(c) is a compact open-source autopilot platform. The latest iterations of the papparazzi platform includes powerful microprocessor ($> 600Mhz$). However, as of the inception of this work the Paparazzi platform was based on a slower ARM microcontroller ($< 32Mhz$) system and therefore not considered for use. Moreover, both the Ardupilot and Paparazzi platforms used low-quality MEMS sensors that have larger systemic biases in measurements.

As an appropriate commercially available autopilot platform does not exist, a custom autopilot system was designed for the vehicles employed in this work. The autopilot design is based on the Paparazzi system however it uses a better suite of MEMS sensors. In addition to the microcontroller found on earlier iterations of the Paparazzi platform, the autopilot designed here also includes a more powerful microprocessor ($800Mhz, 512MB$ RAM) running Linux to aid in more computationaly intensive and high bandwidth communication operations. The addition of the microprocessor also makes the software architecture flexible as software modules can be run on the microcontroller or the microprocessor depending on the computational intensity and real-time performance requirements. The microcontroller is more suited for operations that require guaranteed timing (such as controller algorithms) and while the microprocessor can handle more computationally heavy operations such as high bandwidth communication. The microprocessor also allows for further development

of more complex autonomy software (mapping, planning and related vision algorithms). Figure 4.2 shows the final architecture designed for the autopilot system.

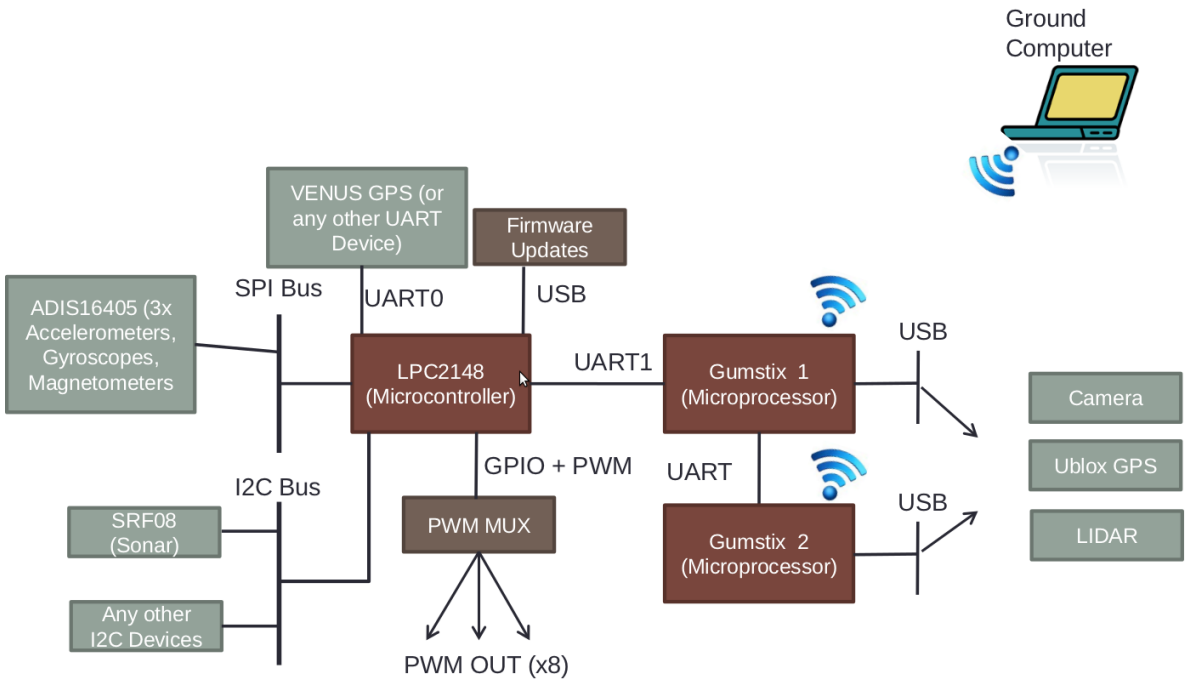

Figure 4.2: UWMAV Autopilot Framework

Figure 4.2 shows the selected sensor components, microcontrollers, microprocessors and the communication systems that connect all the components. The autopilot has a $32Mhz$ Phillips ARM LPC2148 microcontroller and two Gumstix Cortex A8 $800Mhz$ microprocessors to satisfy all the required computing needs. The system uses an Analog Devices IMU as its primary sensor. Additional sensors can be added to the available device communication buses, I2C, SPI and UART for the microcontroller and/or USB on the Gumstix. The actuators of a rotorcraft can be controlled onboard by the PWM system, or the other communication methods available (I2C, SPI and UART) depending on the requirements of the rotorcraft. The Gumstix processors are equipped with Wifi cards that enable wireless communication with the autopilot.

The above system is brought together on a single PCB to ensure the system remains compact. This PCB design was carried through multiple prototyping cycles to ensure electrical stability. The final product is shown in Figure 4.3.

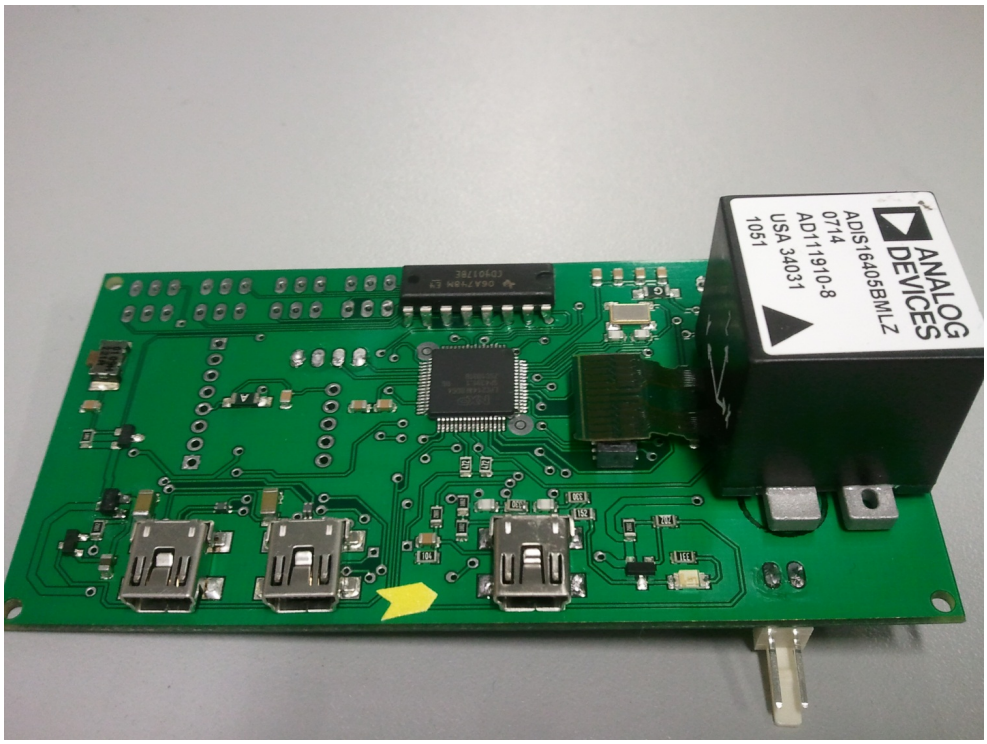

Figure 4.3: UWMAV Autopilot

The UWMAV autopilot can now be installed on various rotorcraft to create autonomous flight craft that provide the required software capabilities and sensor systems to test various controllers and potentially expand to further autonomous behaviour.

4.2 Nonlinear Controllers on the MikroKopter Quadrotor

The quadrotor controller developed in this work needs to be tested on a real helicopter platform. For this, a custom quadrotor platform using the UWMAV Autopilot platform is constructed. A standard quadrotor platform such as the MikroKopter (Figure 4.4(a)) provides a capable mechanical platform and has been employed by previous studies in control systems [36]. Given these previous successes, the Mikrokopter framework is employed along with the UWMAV Autopilot developed before to construct a Quadrotor testbed. The MikroKopter framework uses custom designed brushless motors for actuating the rotors. These motors are controlled by onboard motor controllers designed by MikroKopter. The quadrotor also has an onboard Autopilot system that is interfaced to the motor controllers using the I2C bus. In this work, the MikroKopter autopilot is replaced with the UWMAV Autopilot platform shown in Section 4.1 so as to allow for custom controllers. However, the MikroKopter autopilot is kept in the system as a backup system. The UWMAV Autopilot is mounted onto the Quadro XL platform and the I2C bus on the UWMAV Platform is used to control the brushless motors of the vehicle. Figure 4.4(b) shows the complete system with the UWMAV Autopilot mounted onto the Quadro XL Platform.

4.2.1 Orientation Estimation

The controllers developed in Section 3 assume perfect knowledge of the orientation of the vehicle. However, the UWMAV Autopilot's onboard IMU is equipped with 3 gyroscopes, 3 accelerometers and 3 magnetometers. The gyroscopes provide a measurement of the rotation rates of the quadrotor, the accelerometers measure the vehicle accelerations and can also aid in the measurement of the direction of gravity. The magnetometers measure the orientation of the vehicle with respect to the earth's magnetic field. However, these measurements have a few different sources of error,

- The gyroscopes are known to have signficant biases in the rate measurements

(a) Stock Mikrokopter Quadro XL being using for Aerial Photography

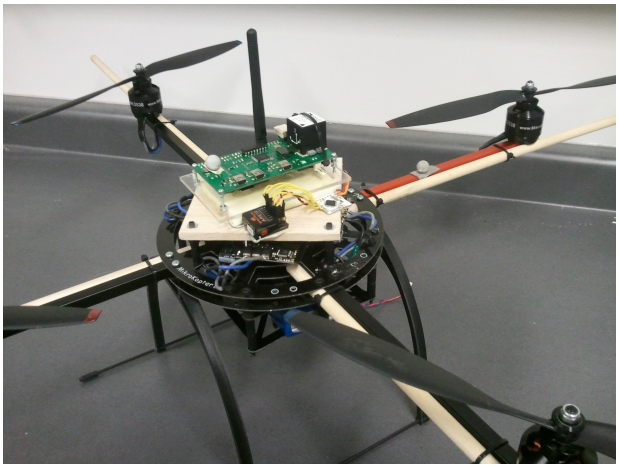

(b) Quadrocopter Testbed using the Mikrokopter and UWMAV Autopilot

Figure 4.4: Quadrotor Testbed

- In order to accurately measure the gravity vector using the accelerometers, the body must experience no other sources of acceleration.
- The magnetometers are prone to large amounts of error due to electrical disturbance caused by the quadrotor motors and related electrical systems.
- Vibrations during flight are a large source of high frequency noise to all measurements from the IMU.

In the period of a single flight, the gyroscopic biases are assumed to be constant. In the first three seconds of flight (before takeoff), the quadrotor is assumed to be static at which time the gyroscopic biases are measured and removed from future measurements. Incorporating magnetometers requires extensive electro-magnetic disturbance studies that is deemed to be outside the scope of this work. The combination of accelerometers and gyroscopes allows us to accurately measure the roll, pitch, roll rate, pitch rate and yaw rate of the vehicle. An accurate measurement of yaw can be acquired through external sources (vision algorithms, indoor positioning systems etc.). In order to combine all the sensor information into one accurate estimate of the orientation, a kinematic Extended Kalman Filter (EKF) is employed. This EKF is also used to suppress the effect of vibration and occasional errors introduced into the measurement of the gravity vector due to quadrotor body accelerations. The EKF is used to estimate the orientation state namely,

$x = \begin{bmatrix} \phi & \theta & \psi & p & q & r \end{bmatrix}^T$. The motion model of the EKF assumes constant acceleration and incorporates the rotation between body angular rates measured by the gyroscopes and the euler rates that are part of the state as shown in Equation (3.3). This can be summarized as,

$$\dot{x} = f(x) \tag{4.1}$$

$$= \begin{bmatrix} \dot{\phi} \\ \dot{\theta} \\ \dot{\psi} \\ \dot{p} \\ \dot{q} \\ \dot{r} \end{bmatrix} = \begin{bmatrix} 0 & 0 & 0 & 1 & \sin(\phi)\tan(\theta) & \cos(\phi)\tan(\theta) \\ 0 & 0 & 0 & 0 & \cos(\phi) & -\sin(\phi) \\ 0 & 0 & 0 & 0 & \frac{\sin(\phi)}{\cos(\theta)} & \frac{\cos(\phi)}{\cos(\theta)} \\ 0 & 0 & 0 & 0 & 0 & 0 \\ 0 & 0 & 0 & 0 & 0 & 0 \\ 0 & 0 & 0 & 0 & 0 & 0 \end{bmatrix} \tag{4.2}$$

Given the sensor suite the measurements fed into the EKF are,

$$y = h(x) = \begin{bmatrix} \cos\theta \sin\phi \\ \sin\theta \\ p \\ q \\ r \end{bmatrix} = \begin{bmatrix} \frac{y_{acc}}{g} \\ \frac{x_{acc}}{g} \\ p_{meas} \\ q_{meas} \\ r_{meas} \end{bmatrix} \tag{4.3}$$

where, y_{acc} and x_{acc} are acceleration measurements and p_{meas}, q_{meas}, and r_{meas} are the body rate measurements from the gyroscopes. The measurement equations of roll (θ) and pitch(ϕ) above are based on a general aircraft model. However, in a quadrotor, this measurement model is not always correct. When a quadrotor experiences a roll and/or pitch motion, it also accelerates in the body x and/or y axes. This acceleration nullifies the measurement shown in Eqn (4.3). However, in the case of near hover flight, on average, the measurement model shown in Eqn. (4.3) will provide accurate results as evident in the results shown in Figure 4.5.

The dynamics in Eqn. (4.1) and Eqn (4.3) are linearized about the current state as required by the the EKF framework using the pre-calculated Jacobian matrices,

$$J_x = \frac{\partial f(x)}{\partial x} \tag{4.4}$$

$$H_x = \frac{\partial h(x)}{\partial x} \tag{4.5}$$

The above system is then implemented onboard the UWMAV Autopilot using the EKF algorithm [11]. The filter is discretized to run at 100Hz and implemented on the micro-controller.

In order to verify that the designed EKF is working as expected, the orientation estimates are compared to those generated by an Optitrack motion capture system. The Optitrack system uses IR cameras to offer highly accurate estimates of the position and orientation of a body based on triangulation of IR markers placed on the body. These IR markers are strategically placed on the quadrotor body and the quadrotor is flown with the stock MikroKopter controller. Figure 4.5 presents the result of such a flight and demonstrates that the Kalman filter output closely tracks the presumed ground truth measurements from the Optitrack and that the orientation estimator is adequately accurate to be used for control tests onboard the quadrotor.

4.2.2 Quadrotor System Identification

The feedback linearized controller proposed in Section 3 assumes that two sets of parameters can be determined before flight:

- The controllers assume that the body forces and torques described in Section 3.1.5 are controllable. However, the MikroKopter framework only provides control over motor speeds. For accurate control of the body forces and torques, accurate knowledge of the parameters k_i and c described in Eqn (3.16) and Eqn (3.17) respectively, is required.
- The body mass (m) and inertia parameters (I_x, I_y, and I_z) are also assumed to be known.

The constant, k_i is the aerodynamic constant that relates the motor input to the thrust generated by the rotors. It depends on the blade geometry and the electronic motor input. In an effort to accurately estimate this parameter, the quadrotor platform is mounted on a scale as shown in Figure 4.6. The scale provides an accurate estimate of the mass (m) of the aircraft.

As the motor input is varied, the scale provides an estimate of the amount of thrust generated by the quadrotor. The motor input can be systematically varied to construct a dataset that can provide an estimate of the constant k_i. However, when the quadrotor attempts to generate thrust close to the ground, as in Figure 4.6, the thrust study will be affected by the rotor backwash from the ground (ground effects) as described in Section 3.1.4. As described before, modelling and predicting the affect of rotor downwash can be quite complex. Moreover, an alternate thrust study stand that minimizes the effect of rotor downwash is outside the scope and resources of this work. The affect of the rotor downwash

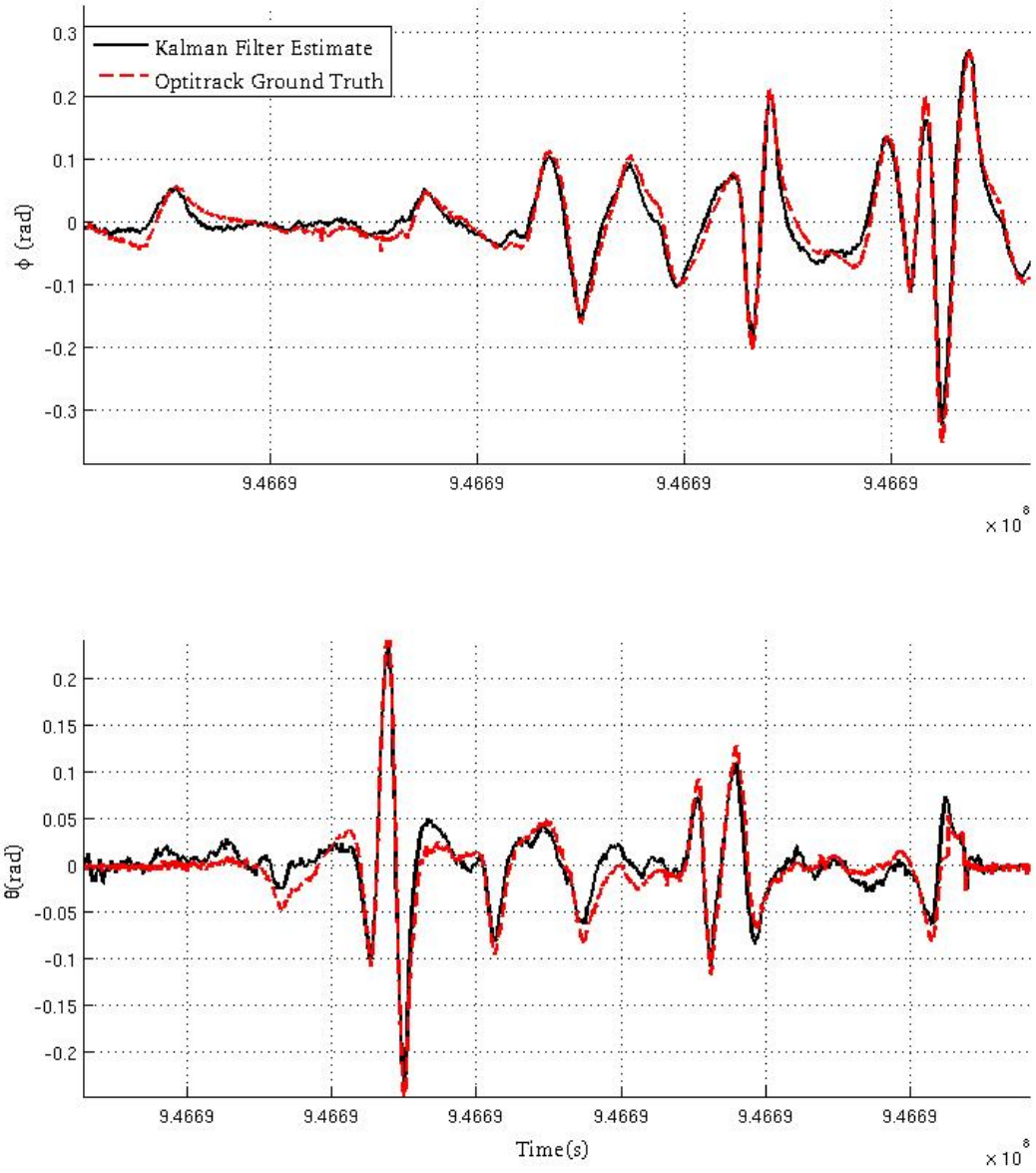

Figure 4.5: Onboard Orientation Estimation System Output

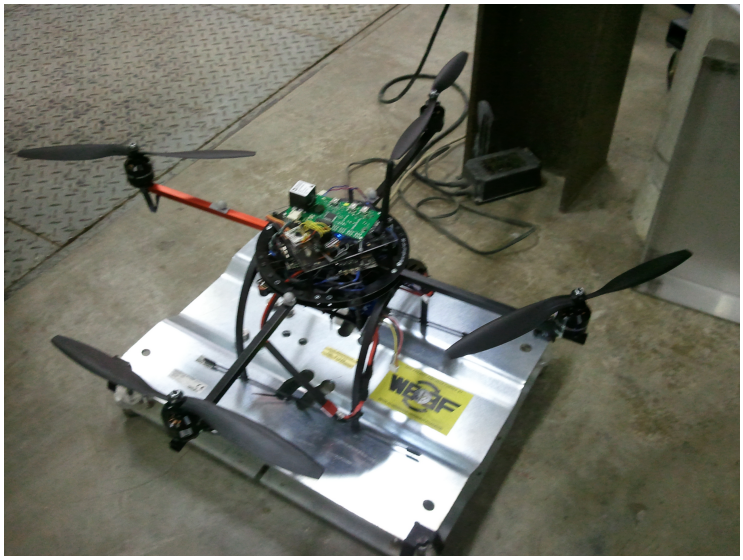

Figure 4.6: Quadrotor platform mounted on a Scale for thrust study

on the thrust study will create a disturbance in the controller as the forces generated by the rotor in flight will be lower than the expected value. The controllers must be able to reduce the affect of this disturbance.

As the constant, k_i, depends on blade geometry, two tests, one with a 12 inch diameter blade and the other with a 13 inch diameter blade is carried out. The result of this thrust test is shown in Figure 4.6. Figure 4.6 also shows the results of a quadratic interpolation on both rotor sizes. As guided by the relationship in Eqn (3.11), the larger rotor generates more thrust for the same applied voltage and is therefore more efficient. Moreover, the quadratic fit can be seen to be accurate and the constant k_i can be retrieved from this fit. The exact values of each of the parameters is summarized in Table 4.1. The parameter c relates the motor speed to the torque generated about the body z axis (to control the yaw of the vehicle). This parameter is retrieved from previous system identification work on fixed pitch rotor systems [8] and scaled to the appropriate rotor size.

Finally, the inertia of the vehicle is estimated using some simplifying assumptions. The central hub and the motors of the vehicle are approximated to circular cylinders and the rods are approximated to be thin rods. This inertia is transferred to be about the x, y and z axis using the parallel axis theorem. The final inertia value used for controller formulation are shown in Table 4.1.

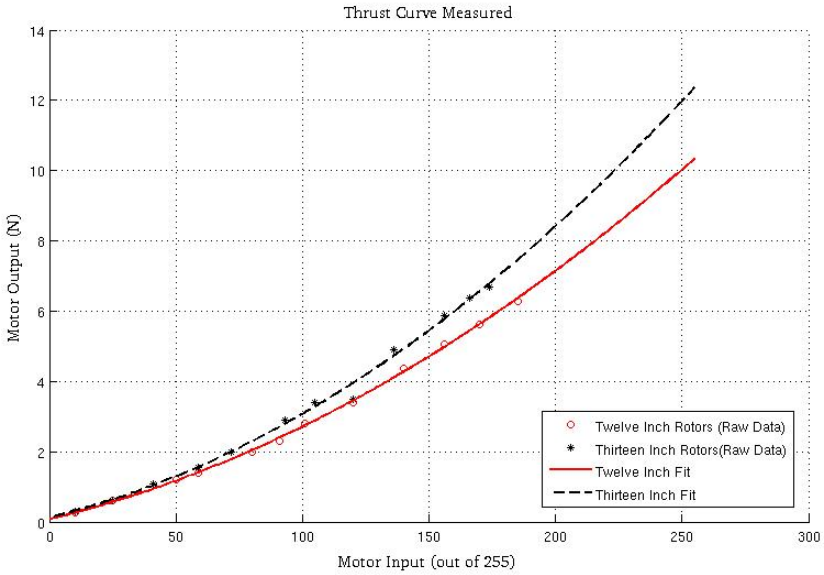

Figure 4.7: Thrust Study Results

Parameter	value
k_i	0.00011952 N
c	0.00001106 N
m	1.555 kg
I_x	0.00294 $kg^2.m^2.rad$
I_y	0.00294 $kg^2.m^2.rad$
I_z	0.05607 $kg^2.m^2.rad$

Table 4.1: Quadrotor Parameters Used

4.2.3 Controller Results

The inner loop controllers described in Section 3 are implemented onboard the UWMAV autopilot on the system shown in Figure 4.4(b). The controllers are formulated using the parameters shown in Table 4.1 and run real time on the microcontrollers. The continuous time dynamics of the controllers shown in Eqn (3.43) and Eqn (3.74), are approximated by running an euler approximation of the continuous controller at 100Hz. The parameters and gains of the controllers are tuned to provide reliable and stable results. This controller setup is used to fly the helicopter while assessing performance. Figure 4.8 shows the quadrotor mid flight.

Figure 4.8: UWMAV Autopilot mid flight on the Mikrokopter

The tracking volume available from the Optitrack indoor positioining system is small. Therefore, quadrotor flights using the more complex input orientation trajectories shown in Section 3 are impossible to safely reproduce. In an effort to assess the reaction of the controllers under more complex sinusoidal trajectories, the quadrotor is placed in a custom test bench that constrains the position movement of the aircraft while allowing it to pitch or roll with minimal additional torque. Figure 4.9 shows the quadrotor in this constrained testbench.

With the quadrotor in this constained testbench, a sinusoidal trajectory can be safely

Figure 4.9: Quadrotor in a constrained testbench

commanded of its orientation.

Using the adaptive and non-adaptive feedback linearized controller a sinusoidal pitch trajectory is commanded of the helicopter. The result is shown in Figure 4.10. Figure

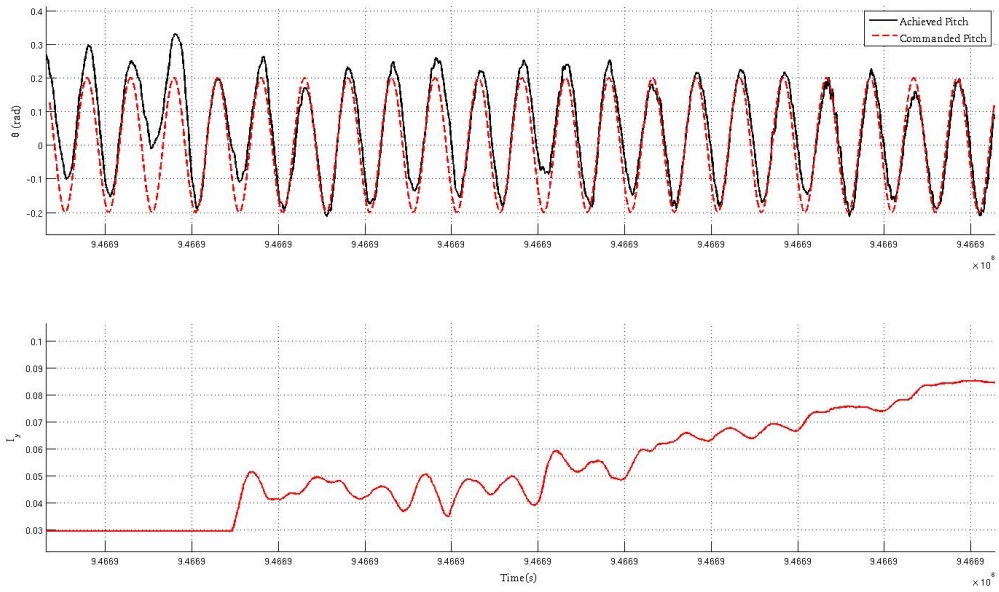

Figure 4.10: Quadrotor Control Results

4.10 shows the commanded and achieved pitch trajectory along with the parameter adaptation of the inertia parameter primarily affecting the pitch direction. In Figure 4.10, the controller is commanded to output a sinusoidal pitch trajectory without the aid of any parameter adaptation for the first 25% of the flight. In this time, a large amount of tracking error (frequently more than 0.05 rad) is noticed. The source of this error could be a combination of,

- Aerodynamic *backdraft* from the surrounding walls around the testbench area.
- Inaccuracies in the parameters idenfitied in Table 4.1.
- Friction from the testbench in the pitch direction of the aircraft.

However, as the inertia parameter is allowed to adapt, the controller is seen to overcome these sources of error to provide improving trajectory tracking. In the last 25% of the flight, the quadrotor is tracking the required trajectory accurately. The parameter I_y in Figure 4.10 settles at over three times the initial value shown in Table 4.1. As described in Section 3, the adaptive controller framework is *direct* and therefore the parameter estimate has settled at a value that is appropriate for the given trajectory and potential sources of error. The parameter may not be universally accurate and may change to a lower value when it is required to track a less aggressive trajectory or when the flight is under the influence of fewer disturbances. This behaviour of the controller, to increase parameter estimates to values larger than required, is visible in Figure 3.17 where the parameters sharply rise to a larger amount to ensure suppression of wind disturbances.

Finally, a major difference between the experimental results and the simulation studies shown in Section 3 can be observed. The simulated parameter response (Figure 3.17 and 3.13) in the inertia direction is sharp, leading to the quadrotor being able to track the required trajectory much faster. However, in the case of the experimental results in Figure 4.10 the parameter reacts slowly, resulting in longer periods of inaccurate tracking. This slower response is likely the result of higher levels of measurement noise and dynamic disturbances.

Chapter 5

Conclusions

Small Unmanned Aerial Vehicles (< 1m) have recently seen a large growth in popularity. Their small size, relatively cheap cost and potential flight capabilities have made them an extremely popular choice in a growing number of industries and applications that have previously been unable to employ unmanned technology. Moreover, recent advances in microcomputer technology and MEMS sensor systems have created a perfect environment for systems like these to flourish.

The fundamental problem with most UAV systems is the safe, robust and reliable flight of the platform in various circumstances. The small size of these vehicles pose a unique set of challenges for the potential users and designers of these vehicles. The shrinking size of the onboard sensor systems inject more noise into the control algorithms. The small physical size of the flight chassis makes the system more susceptible to disturbances from the environment. These factors must be considered and mitigated when designing these platforms for robust and reliable flight. In current literature over the last decade, there have been numerous works in developing linear control methods for sUAV systems. However, recent advancements in microcomputer technology have allowed for more advanced nonlinear algorithms to be implemented onboard these systems. These nonlinear methods promise better results but assume perfect knowledge of the vehicle dynamics. This work intends to discuss and develop these control methods in the context of two different sUAV configurations.

Many different configurations of sUAV's are currently under investigation, with new designs still being made. However, the coaxial helicopter and the quadrotor helicopter configurations are two of the most popular platforms that are being considered or have already been commercialized for use in various applications. The coaxial helicopter dy-

namics rely on a dual-rotor system that makes this configuration compact and easier to control using linear methods due to the damped response around the linear zone of flight. Along with the compactness, the damping of the dynamics makes the coaxial helicopter inherently stable and the dual rotor system makes the power train much more efficient. However, the damping also takes away a lot of the control authority making it difficult to fight wind and/or follow aggressive trajectories.

The quadrotor platform is better suited for providing a larger amount of control authority to be able to suppress the effect of external disturbances. It uses four rotors to create thrust and uses the difference in thrust between the various rotors to create moments about the roll, pitch and yaw directions. The simpler set of quadrotor dynamics means the vehicle does not require a complex mechanical geartrain system making quadrotor platforms cheaper and easier to maintain. Moreover, the small rotor size (compared to traditional helicopters) injects less kinetic energy in the system which ensures fewer catastrophic crashes. However, the extra control authority comes at the price of nonlinearities being present in regular flight. The vehicle does not have the damping that a coaxial helicopter possesses and therefore any controller designed for this system must contain knowledge of these faster nonlinearities and/or use suitable control methods to regulate the vehicle.

In terms of controller design, due to its inherent damping and stability, only linear methods are considered for the coaxial helicopter system. A full set of dynamics is derived based on simplifications from earlier work. These dynamics are then decoupled so that four seperate PID systems can control the roll, pitch, yaw and height of the vehicle while minimizing interference. The dynamics are linearized about hover and an optimal control strategy based on quadratic costs (Linear Quadratic Regulation) is also designed. Finally, to test the applicability of frequency domain designs a Robust H_∞ method is also devised. The LQR control method is shown to be superior to PID control methods in suppressing the cross-channel interactions in coaxial helicopter simulation flights. However, the simulation studies also showed that the H_∞ control method is better at suppressing higher frequency wind disturbances frequently experienced by sUAV platforms. Moreover, the H_∞ controller is shown to be able to better track aggressive position trajectories.

The quadrotor control problem is more complicated due to the inherent nonlinearities in the flight of the quadrotor. In this work, the dynamics of the quadrotor are derived using various current works. In an effort to provide adequate comparison, an LQR control method is designed to control the dynamics of the quadrotor. Various nonlinear methods are considered, however the popular feedback linearization method is deemed to show the most promise for usage in quadrotor platforms. Based on the recommendations of some previous work, the feedback linearization plant is decoupled into an inner and outer loop.

The feedback linearization method is simulated and shown to be superior to the LQR method devised in this work.

Feedback linearization, like most nonlinear methods, requires accurate knowledge of the quadrotor plant parameters. These parameters are difficult to accurately estimate and may even change during the course of a flight. Using simulation studies, inaccuracies in plant parameters are shown to be detrimental to the performance of feedback linearization methods. To counteract the effects of these inaccuracies a direct adaptation law is derived based on some previous work on mechanical manipulators to run parallel to the feedback linearization method. This adaptation law is directly driven by trajectory tracking errors and modifies the plant parameters to suppress these errors. As the adaptation law is driven by tracking errors, it may modify the parameters so as to increase or decrease the *effective* gains used by the feedback linearization method to suppress all sources of error (not just parameter errors). This adaptation method is shown to accurately estimate the correct parameters in cases with no other sources of disturbances. It is also shown to estimate changes in plant parameters during flight to maintain stable flight of the quadrotor. Finally, the disturbance rejection characteristics of the controller are also tested. In general, the feedback linearization method is shown to improve under all scenarios when coupled with the results of the parameter adaptation law.

Finally, a custom autopilot and helicopter testbed is constructed to test the quadrotor controllers. Various estimation and softare systems are developed and tested to support the proper functioning of the controller. The feedback linearization controller is implemented online and tested with and without the adaptation law on a custom test bench. The custom test bench constrains the flight of the quadrotor which allowed the quadrotor platform to safely follow a complex inner loop roll or pitch trajectory. The trajectory tracking is shown to substantially improve when the plant parameters are allowed to adapt according to the adaptation law derived in this work. Moreover, the plant parameters are shown to grow significantly to suppress the larger sources of disturbances that appeared in real flight. This illustrates the advantage of a *direct* adaptive control method that has the flexibility to change the parameters to reduce tracking error ultimately ensuring safer, more reliable and accurate flight.

References

[1] S.A. Al-Hiddabi. Quadrotor control using feedback linearization with dynamic extension. In *Mechatronics and its Applications, 2009. ISMA'09. 6th International Symposium on*, pages 1–3, Sharjah, UAE, 2009.

[2] C. Anderson. How I Accidently Kickstarted the Domestic Drone Boom, June 2012.

[3] A. Benallegue, A. Mokhtari, and L. Fridman. Feedback linearization and high order sliding mode observer for a quadrotor UAV. In *Variable Structure Systems, 2006. VSS'06. International Workshop on*, pages 365–372. IEEE, 2006.

[4] S. Bouabdallah. *Design and control of quadrotors with application to autonomous flying*. PhD thesis, Lausanne Polytechnic University, 2007.

[5] S. Bouabdallah, A. Noth, and R. Siegwart. PID vs LQ control techniques applied to an indoor micro quadrotor. In *International Conference on Intelligent Robots and Systems 2004*, volume 3, pages 2451 – 2456 vol.3, 2004.

[6] S. Bouabdallah and R. Siegwart. Backstepping and sliding-mode techniques applied to an indoor micro quadrotor. In *International Conference on Robotics and Automation 2005*, pages 2247 – 2252, april 2005.

[7] S. Bouabdallah and R. Siegwart. Full control of a quadrotor. In *International conference on intelligent robots and systems*, pages 153–158. Ieee, 2007.

[8] S. Bouabdallah, R. Siegwart, and G. Caprari. Design and control of an indoor coaxial helicopter. In *RSJ International Conference on Intelligent Robots and Systems 2007*, pages 2930–2935. IEEE, 2007.

[9] A. R. S. Bramwell, George Done, and David Balmford. *Bramwell's Helicopter Dynamics*. Butterworth-Heinemann, Oxford, England, 2nd edition, 2001.

[10] A. E. Jr. Bryson and Y. C. Ho. *Applied Optimal Control: Optimization, Estimation, and Control*. John Wiley & Sons, New York, NY, 1975.

[11] W. Burgard, D. Fox, and S. Thrun. Probabilistic robotics, 2005.

[12] Li Chen and Phillip McKerrow. Modelling the lama coaxial helicopter. In *Australasian Conference on Robotics and Automation 2007*, Brisbane, Australia, 2007. Australian Robotics and Automation Association.

[13] C.P. Coleman. A survey of theoretical and experimental coaxial rotor aerodynamic research. Technical Report 3675, NASA Ames Research Center, March 1997.

[14] I.D. Cowling, O.A. Yakimenko, J.F. Whidborne, and A.K. Cooke. A prototype of an autonomous controller for a quadrotor uav. In *European Control Conference*, pages 1–8, 2007.

[15] J.J. Craig, P. Hsu, and S.S. Sastry. Adaptive control of mechanical manipulators. *The International Journal of Robotics Research*, 6(2):16, 1987.

[16] A. Das, K. Subbarao, and F. Lewis. Dynamic inversion with zero-dynamics stabilisation for quadrotor control. *Control Theory & Applications, IET*, 3(3):303–314, 2009.

[17] J. Doyle. Guaranteed margins for LQG regulators. *IEEE Transactions on Automatic Control*, 23(4):756–757, 2002.

[18] A. Dzul, T. Hamel, and R. Lozano. Modeling and nonlinear control for a coaxial helicopter. In *IEEE International Conference on Systems, Man and Cybernetics 2002*, Hammamet, Tunisia, October 2002.

[19] J. Etele. Overview of wind gust modelling with application to autonomous low-level uav control. Technical Report CR 2006-221, Defence Research and Development Canada - Ottawa, November 2006.

[20] Bernard Etkin. *Dynamics of Atmospheric Flight*. John Wiley & Sons, Inc., New York, 1972.

[21] C.D. Hendrix, M.J. Veth, and R.W. Carr. LQG Control Design for a Hovering Micro Air Vehicle Using an Optical Tracking System. In *IEEE Aerospace Conference 2009*, pages 1 –14, Big Sky, Montana, USA, March 2009.

[22] G.M. Hoffmann, H. Huang, S.L. Waslander, and C.J. Tomlin. Quadrotor helicopter flight dynamics and control: Theory and experiment. In *AIAA guidance, navigation, and control conference 2007*, volume 4, 2007.

[23] G.M. Hoffmann, H. Huang, S.L. Waslander, and C.J. Tomlin. Precision flight control for a multi-vehicle quadrotor helicopter testbed. *Control Engineering Practice*, 2011.

[24] R.V. Jategaonkar. *Flight vehicle system identification: a time domain methodology*. American Institute of Aeronautics and Astronautics, 2006.

[25] H.K. Khalil and JW Grizzle. *Nonlinear systems*, volume 3. Prentice Hall New Jersey, 2002.

[26] D. Lee, H. Jin Kim, and S. Sastry. Feedback linearization vs. adaptive sliding mode control for a quadrotor helicopter. *International Journal of Control, Automation and Systems*, 7(3):419–428, 2009.

[27] J.G. Leishman. *Principles of helicopter aerodynamics*. Cambridge Univ Pr, 2006.

[28] T. Madani and A. Benallegue. Backstepping Control for a Quadrotor Helicopter. In *Intelligent Robots and Systems, 2006 IEEE/RSJ International Conference on*, pages 3255 –3260, 2006.

[29] D. Mellinger, Q. Lindsey, M. Shomin, and V. Kumar. Design, modeling, estimation and control for aerial grasping and manipulation. In *Intelligent Robots and Systems (IROS), 2011 IEEE/RSJ International Conference on*, pages 2668 –2673, sept. 2011.

[30] B. Mettler. *Identification Modeling and Characteristics of Miniature Rotorcraft*. Kluwer Academic Publishers, Norwell, MA, USA, 2003.

[31] M.Huang, B.Xian, C.Diao, K.Yang, and Y.Feng. Adaptive tracking control of underactuated quadrotor unmanned aerial vehicles via backstepping. In *American Control Conference (ACC), 2010*, pages 2076 –2081, 30 2010-july 2 2010.

[32] Military Specification. Flying Qualities of Piloted Airplanes. Technical Report U.S. Military Specification MIL-F-8785C.

[33] P. Pounds, R. Mahony, and P. Corke. Modelling and control of a quad-rotor robot. In *Australasian conference on robotics and automation 2006*, Auckland, NZ, 2006.

[34] Robb L. Raymond. Hybrid helicopters: compounding the quest for speed. *Journal of the American Helicopter Society*, 52:30–54, 2006.

[35] A. Ruddell. Advancing Blade Concept Development Test Program. *Journal of the American Helicopter Society*, 22(13), 1977.

[36] I. Sa and P. Corke. Estimation and control for an open-source quadcopter. In *Australasian Conference on Robotics and Automation 2011*, 2011.

[37] D. Schafroth, C. Bermes, S. Bouabdallah, and R. Siegwart. Modeling, System Identification and Robust Control of a Coaxial Micro Helicopter. *Control Engineering Practice*, 18(7):700–711, 2010.

[38] S. Skogestad and I. Postlethwaite. *Multivariable Feedback Control: Analysis and Design*. John Wiley & Sons, Inc, New York, 1996.

[39] Hongqiang Wang, Daobo Wang, Xinwen Niu, and Haibin Duan. Modeling and hover control of a novel unmanned coaxial rotor/ducted-fan helicopter. In *IEEE International Conference on Automation and Logistics 2007*, pages 1768–1773, Jinan, China, August 2007.

[40] K. Watanabe, Y. Yoshihata, Y. Iwatani, and K. Hashimoto. Image-based visual PID control of a micro helicopter using a stationary camera. In *International Conference on Instrumentation, Control and Information Technology 2007*, pages 3001–3006, Takamatsu City, Kagawa, Japan, September 2007.

[41] M.F. Weilenmann, U. Christen, and H.P. Geering. Robust helicopter position control at hover. In *AACC American Control Conference 1994*, Baltimore, MD, July 1994.

[42] B. Whitehead and S. Bieniawski. Model Reference Adaptive Control of a Quadrotor UAV. In *Guidance Navigation and Control Conference 2010*, Toronto, Ontario, Canada, 2010. AIAA.

[43] S. Wu, Z. Zheng, and K.Y. Cai. Indoor autonomous hovering control for a small unmanned coaxial helicopter. In *8th IEEE International Conference on Control and Automation 2010*, pages 267–272. IEEE, 2010.

[44] R. Xu and U. Ozguner. Sliding mode control of a quadrotor helicopter. In *Decision and Control, 2006 45th IEEE Conference on*, pages 4957 –4962, dec. 2006.

[45] S. Zaloga and D. Rockwell. UAV Market Set for 10 Years of Growth, January 2011.

[46] W. Zeng, B. Xian, C. Diao, Q. Yin, H. Li, and Y. Yang. Nonlinear adaptive regulation control of a quadrotor unmanned aerial vehicle. In *Control Applications (CCA), 2011 IEEE International Conference on*, pages 133 –138, 2011.